The Ljubija geothermal field: A herald of the Pangea break-up (NW Bosnia and Herzegovina)

Ladislav A. Palinkaš[1], Sibila Borojević Šoštarić[2], Sabina Strmić Palinkaš[3], Walter Prochaska[4], Zoltan Pécskay[5], Franz Neubauer[6] and Jorge E. Spangenberg[7]

[1]University of Zagreb, Faculty of Science, Institute of Mineralogy and Petrology, Horvatovac 95, HR-10000, Zagreb, Croatia (corresponding author: lpalinkas@geol.pmf.hr, phone: ++385 1 3361189)
[2]University of Zagreb, Faculty of Mining, Geology and Petroleum Engineering, Department of Mineralogy, Petrology and Mineral Resources, Pierottijeva 6, Zagreb, Croatia
[3]University of Tromsø, Faculty of Science and Technology, Department of Geology, Dramsvegen 201, N-9037 Tromsø, Norway
[4]Institute für Geowissenschaften, Montanuniversität, Peter-Tunner-Strasse, A-8700, Leoben, Austria
[5]Hungarian Academy of Sciences, Institute of Nuclear Research, Bém tér 18/C, H-4001, Debrecen, Hungary
[6]University of Salzburg, Department of Geography and Geology, Hellbruner Str. 34, A-5020, Salzburg, Austria
[7]Institute of Earth Surface Dynamics, Bâtiment GEOPOLIS, CH-1015 Lausanne, Switzerland

3-30 26 Figs. 2 Tabs. doi: 10.4154/gc.2016.02

Article history:
Received December 07, 2015
Revised and accepted January 26, 2016
Avaliable online February 29, 2016

Keywords: Siderite-barite-polysulphide deposits, Dinarides, Ljubija, Permian, zebra texture siderite, early intracontinental rifting, Pangea break-up, geothermometry, geochronology.

ABSTRACT

The Ljubija ore deposits are the *loci typici* of siderite-barite-polysulphide deposits within the Inner Dinarides, Gemerides and Eastern Alps. Numerous sites of ore outcrops, smaller or larger ore bodies of mineralization, consisting of Fe carbonates, sulphides, barite and fluorite are scattered over an area of 150 square km. The half billion tons of iron ore resources occur as replacement in dolostones and limestones, and as open-space fillings (veins, veinlets) in phyllites and sandstones. The genesis of the Ljubija ore deposits has been explained as (i) syngenetic sedimentary-exhalative, (ii) hydrothermal-metasomatic in Middle Triassic time or (iii) hydrothermal replacement of sedimentary carbonates in Permian time. Basically two alternatives Variscan or Alpine metallogeny, frame the time of genesis from the Middle Carboniferous to the Middle Triassic. Genetic interpretation of the Ljubija ore deposits required convincing arguments based on recent achievements of plate tectonics. This contribution presents a set of new data on ore petrology, geochemistry, geology and time of formation. The Ljubija ore field could justifiably be termed the "Ljubija geothermal field", due to its areal extent and the thermal characteristics of numerous ore deposits and occurrences within the Sana-Una Palaeozoic terrain. The Ljubija geothermal field marks the first signs of thermal instability of Pangea, revealing its breakdown along the deep fractures and heralding incipient intracontinental rifting, the first phase of the new Alpine Wilson cycle. The research reveals novel data on the P-T-X characteristics of ore forming fluids (microthermometry, ion chromatography, Raman spectrometry), sulphur isotopes, maturity of organic matter by vitrinite reflection, and age determination by $^{40}Ar/^{39}Ar$ and K-Ar methods. It adopts argumentatively all the estimated research parameters that constrain a justified genetic model.

1. INTRODUCTION

The Ljubija ore deposits are located in Northwest Bosnia and Herzegovina (44.55˚N, 16.3˚E; Fig. 1), at the margin of the Mesozoic carbonate platform, within the Sana-Una river Palaeozoic terrain, a part of the Inner Dinarides. Numerous sites of ore outcrops represent smaller or larger bodies of mineralization, consisting of Fe carbonate, sulphide minerals, barite and fluorite over an area of 150 square km.

According to written documents, iron ore excavation in this area began in the years before Christ. The first miners were Phoenicians and Illyrians. Romans excavated and smelted iron ore for over 400 years in Ljubija and they transported iron bars by road and the Sana, Una, Sava, and Danube rivers to places for further processing. In the middle ages, iron ore was smelted by the Turks, as confirmed by the remains of primitive smelting plants in this area. In 1916, during World War I., modern mining of iron was started by the Austro-Hungarian monarchy and the production of iron ore has been ongoing for 99 years intermittently under the changing geopolitical divisions in this part of the Balkans. The potential reserves of iron ore have been estimated at 500 million tonnes with an average Fe content of 40-49 %. There are two types of iron ore, Fe-carbonates, siderites and ankerites, and secondary oxide ores with limonite, in proportions of approx. 1:1 (CVIJIĆ, 2004).

Modern industrial mining in the Ljubija ore field (Adamuša ore deposit) began however, as a lead-zinc mine, and was temporarily aimed at mining barite and fluorite as well (CVIJIĆ, 2001; CVIJIĆ, 2004; GRUBIĆ & CVIJIĆ, 2003). The Ljubija ore field includes four opencast mines (Adamuša, Tomašica, Omarska, and Vidrenjak) in an area of about 120 km^2. Besides iron, several other commodities such as zinc, lead, barite, and fluorite were also exploited.

The siderite ore occurs as a replacement in dolostones and limestones, and as open-space fillings (veins, veinlets) in phy-

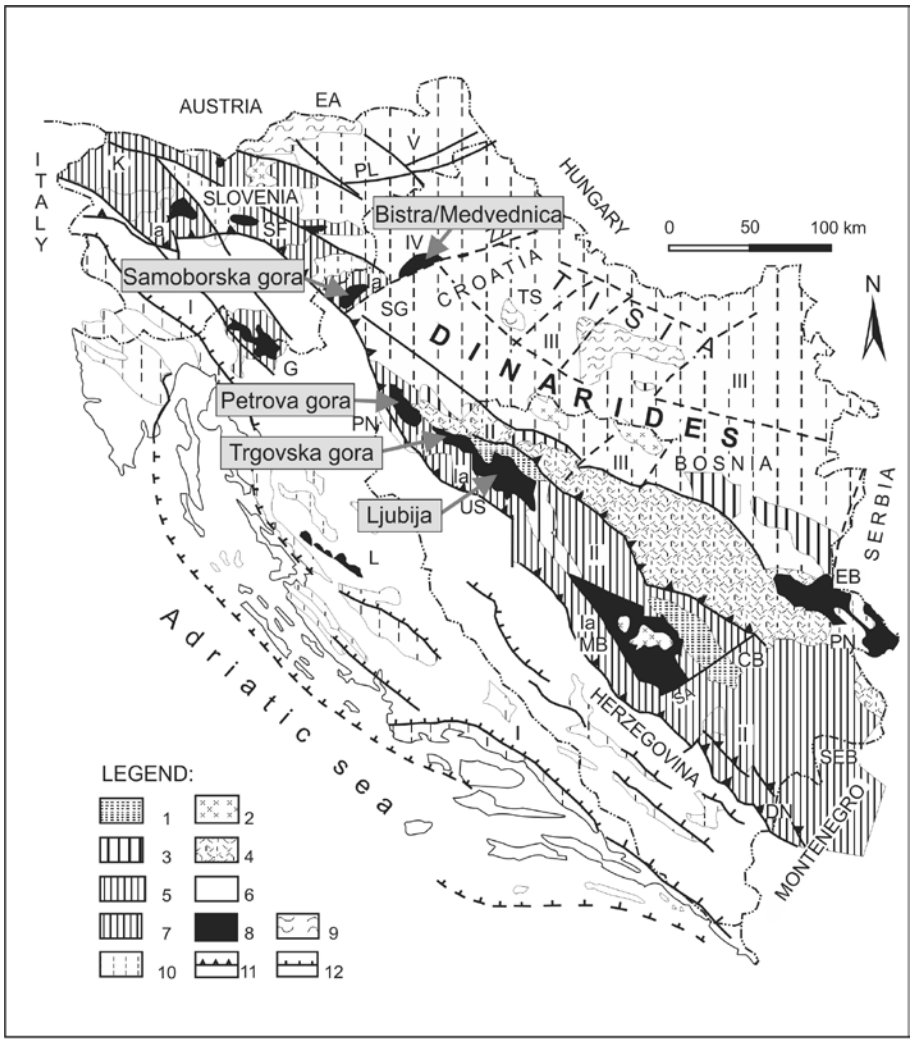

Figure 1. Geological map of the Northwestern and Central Dinarides with the position of the siderite-barite-polysulphide deposits within the Upper Palaeozoic formation of the Inner Dinarides, Ljubija ore field, Trgovska gora, Petrova gora, Samoborska gora, Bistra Medvednica Mts. (accommodated on the map after PAMIĆ et al., 1998). (1) Palaeogene-Neogene overstep sequences (2) Palaeogene metamorphics and granitoids, (3) Upper Cretaceous and Palaeogene flysch, (4) Ophiolites, mostly mélange (5) Jurassic-Cretaceous sequences (6) Adriatic-Dinaridic carbonate platform, (7) Allochthonous Triassic sequences, (8) Allochthonous Palaeozoic sequences and rhyolites, (9) Palaeozoic Hercynian metamorphic rocks and granitoids (10) Faults, (11) nappe, (12) Reverse faults, I Outer Dinarides, Ia Sava nappe, II Inner Dinarides, IIa Pannonian nappe, IIb Durmitor nappe, III Pannonian basin, IV Zagorje-Mid-Transdanubian zone, V Eastern Alps. Large faults: PL Periadriatic, ZZ Zagreb-Zemplin.

llites and sandstones, with rare chalcopyrite and pyrite. The replacement ore has occasionally a zebra texture, with rhythmic banding of dark fine-grained and light sparry siderite, galena, sphalerite and quartz as open-space fillings. Large accumulation of limonite occurs as a secondary ore, named „brand".

The genesis of the Ljubija ore deposits has been explained by a few streams of thinking, (i) as a syngenetic sedimentary-exhalative, or as washouts of lateritic crusts in the sedimentary basin from a dry land area in Carboniferous time (JURKOVIĆ, 1961; JURIĆ, 1971; ŠARAC, 1981), as (ii) of hydrothermal-metasomatic origin in Middle Triassic time (CISSARZ, 1951; JANKOVIĆ, 1977), or as (iii) a hydrothermal replacement of sedimentary carbonates in Permian time, recognized by KATZER (1925); and advocated by PALINKAŠ (1988; 1990), PALINKAŠ et al. (2003b) and coworkers BOROJEVIĆ ŠOŠTARIĆ (2004), STRMIĆ PALINKAŠ (2004), and STRMIĆ PALINKAŠ et al. (2009).

The Ljubija deposits are the *loci typici* of the siderite-barite-polysulfide deposits within the Inner Dinarides, Gemerides and Eastern Alps. Previous studies connected the formation of the deposits either to the Variscan or to the Alpine metallogenesis and considered the Middle Carboniferous or Middle Triassic time of formation, respectively. However, the application of modern plate tectonic aspects of ore genesis is necessary for clarifying these controversial views on the origon of the mineralisation.

Variscan or Alpine metallogeny frame the time of genesis from the Middle Carboniferous to the Middle Triassic. Genetic interpretation of the Ljubija ore deposits required, however, convincing arguments based on the recent achievements of plate tectonics. A basic framework of Wilson cycles has been successfully established but difficulties have arisen from unresolved problems such as the time and space boundary between Variscan and Alpine tectogenesis. It was a source of ambiguity in the fundamental research of Ljubija ore genesis. A proper genetic model depends substantially on understanding of the geological evolution of the Dinarides. This contribution presents a set of new data on ore petrology, geochemistry and geology of the Ljubija ore field, or justifiably termed the „Ljubija geothermal field" in this wider sense of meaning, due to its areal extent and thermal characteristics of numerous ore deposits and occurrences within it.

This paper presents new data on the P-T-X characteristics of ore forming fluids (microthermometry, ionic chromatography, laser Raman spectrometry), sulphur isotopes, maturity of organic matter by vitrinite reflection, and age determination by $^{40}Ar/^{39}Ar$ and K/Ar methods. It adopts argumentatively all the estimated research parameters which constrain a justified genetic model.

2. SUMMARY OF PREVIOUS STUDIES ON THE GEOLOGY AND ORIGIN OF THE LJUBIJA ORE DEPOSITS

The first description of the mineralization in the Ljubija basin came from KATZER (1910). He recognized the relationship between the Carboniferous limestone and siderite mineralization as a reaction contact, which was defined more precisely as a result of metasomatism, in his later work (KATZER, 1925). Thermal water enriched in iron bicarbonate, deposited siderite into the crevices of schists and limestones in the form of siderite veins with some sulphides and quartz. The solutions circulating through the networks of interconnected fractures within schists and limestone filled them with siderite. Simultaneously, solutions caused metasomatism of the limestones into siderite and more distantly in fissures as ankerite. Later tectonics cut deposits into blocks and displaced them, into the present geological structure. The only exception, suggesting syngenetic formation, was in Krivaja ore occurrences, in the Tomašica district. CISSARZ (1951) described the Ljubija mineral deposits as hydrothermal deposits of Paleozoic age and related them to deep magmatism. All these descriptions are a short transposition of Katzer's genuine obervations and interpretations.

NÖTH (1952) supposed an intrusive-hydrothermal origin and Upper Palaeozoic age for the siderite veins and irregular ore bodies.

RAMOVIĆ (1957) distinguished three types of mineral deposits in the Ljubija area: (i) siderite veins hosted by Palaeozoic schists and related to metasomatism of limestones intercalated with smaller or larger quantities of clastic material, (ii) metasomatic ore bodies hosted by Palaeozoic limestones and (iii) secondary deposits formed by weathering.

JURKOVIĆ (1961) described Ljubija as marine sedimentary deposits of Upper Carboniferous age. The Fe carbonates, siderite and ankerite, were deposited as mud, together with some contributory clastic detritus, with irregular sedimentary proportions. Iron carbonates were cryptocrystalline and present-day textures were recrystallized through diagenetic processes.

JURIĆ (1971) supported a synsedimentary origin of the Ljubija mineral deposits.

JANKOVIĆ (1987) emphasized the importance of Permo-Triassic intracontinental rifting, with a magmatic paroxysm in the Middle Triassic. This is also the period when volcano-sedimentary deposits, skarns, massive sulphides, mercury deposits, bedded ferromanganese oxides, and MVT deposits were formed in the Dinarides. There is no distinction, however, between Permian early intracontinental rifting and Triassic advanced rifting stages, so the Ljubija deposits remain in the vast group of Triassic deposits. Their subterrestrial nature and lack of contemporaneous magmatism in the area did not attract attention as an argument for genetic modelling and discrimination from other Triassic deposits.

PALINKAŠ et al. (1985, 1988, 1990, 2010) applied a wide spectrum of analytical methods to the siderite-barite-sulphides mineral deposits hosted by Upper Palaeozoic sedimentary complexes of the Inner Dinarides. Special attention was paid to the Ljubija ore deposits. On the basis of fluid inclusion studies in quartz from three distinctive ore textures, e.g. dark massive siderite, zebra texture with dark and light siderite bands, and siderite veins in phyllites and meta-sandstones, the deposits were unambiguously ascertained to be hydrothermal in nature. Boiling of ore forming fluids was recognised in the Žune-Dolinac barite-fluorite ore body in the Ljubija ore field. It was used to reconstruct the depth of ore forming processes within one of numerous barite occurrences. Applied hydrostatic pressure determines variable depths of formation around 100-200 m. Based on the plumbotectonic modeling, PALINKAŠ (1985), suggested a new genetic model with a subterrestrial, hydrothermal convection cell and suggested the Permian as the formation time, related to the *early intracontinental rifting*. The model leaned on the contemporary plate tectonic reconstructions by CHANNEL et al. (1979), HORVATH & D'ARGENIO (1985), KOVACS (1984), and PAMIĆ (1984), which convincingly linked similar deposits along the present day edge of the carbonate platform, Trgovska Gora, Petrova Gora, Samoborska Gora (Croatia; PALINKAŠ et al., 2000, 2001, 2003a, 2010; BOROJEVIĆ ŠOŠTARIĆ et al. (2004, 2009), Rudabanya (Hungary; SZAKALL, 2001), Rudnyani (Slovakia, HURAI et al., 2002) and Erzberg (Austria, PROCHASKA et al., 1997) with an equivalent genesis in time and space.

BOROJEVIĆ ŠOŠTARIĆ (2004), on the basis of fluid inclusion studies, vitrinite reflection, $^{40}Ar/^{39}Ar$ and K-Ar dating supported a genetic model based on the subterrestrial hydrothermal convection cell and Permian time of mineralisation related to early intracontinental rifting events.

STRMIĆ PALINKAŠ et al. (2009) presented an extensive geochemical study of the ore and host rocks and made a significant breakthrough in the interpretation and confirmation of the previous studies. The study was focused on the stable isotope composition of barren and mineralized carbonates ($\delta^{13}C$ and $\delta^{18}O$ values), quartz ($\delta^{18}O$), and sulphur minerals ($\delta^{34}S$), the distribution of major and trace elements, including REE, in barren and mineralized carbonates and surrounding clastics, and organic geochemistry research (total organic carbon, hydrocarbons distribution, isotopic composition of individual alkanes ($\delta^{13}C$), and kerogen ($\delta^{13}C$, $\delta^{15}N$) of barren and mineralized samples.

3. GEOLOGICAL SETTING

3.1. REGIONAL GEOLOGICAL SETTING

The orogenic belt of the Dinarides stretches 700 km along the north-eastern margin of the Adriatic microplates (DERCOURT et al., 1993). In the north, this highly complex folded, thrusted and imbricated belt merges with the Southern Alps and in the southeast it extends into the Hellenides (PAMIĆ et al., 1998). The general strike of the folds, thrusts and knappes in the Central Dinarides is NW–SE, and the transport direction is towards the SW. The main tectonstratigraphic units of the Central Dinarides display a regular zonal pattern from stable Adria to Tisia. The historical division to "External" and "Internal" Dinarides, predates the plate tectonic concept, but it is still useful to discriminate tectonostratigraphic elements belonging to the passive and active Tethyan continental margins, respectively. The Dinaridic Palaeozoic complexes (PCs) occur in the Exter-

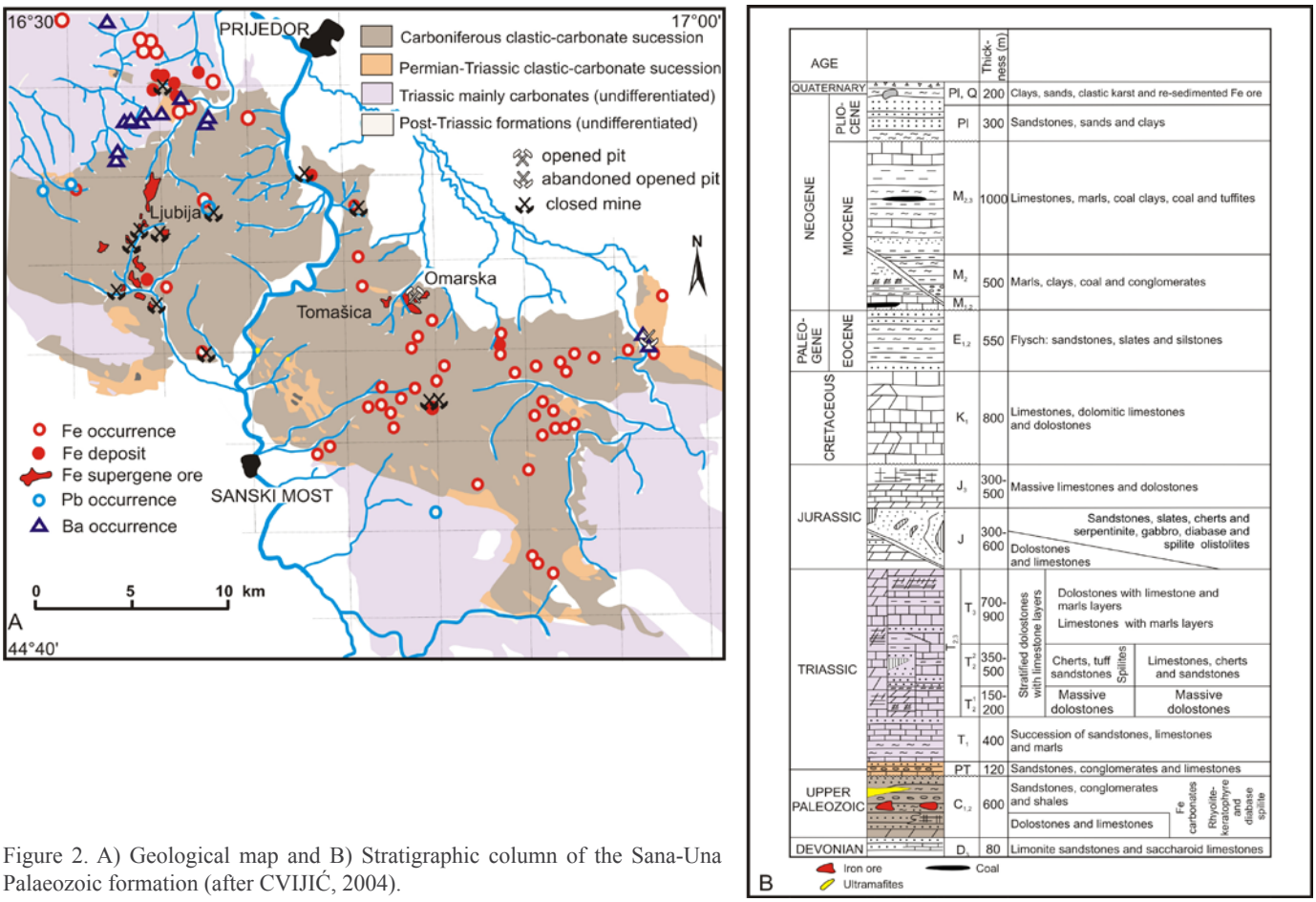

Figure 2. A) Geological map and B) Stratigraphic column of the Sana-Una Palaeozoic formation (after CVIJIĆ, 2004).

nal and Internal Dinarides. The PCs in the External Dinarides, close to or within the carbonate platform, acquired a comparatively autochthonous position relative to their Mesozoic cover. Within the Sava knappe, PCs are disrupted and allochtonous. They can be correlated tectonostratigraphicaly with those in the Southern Alps, and could be related to the passive continental margin of Gondwana. The Palaeozoic formations within a carbonate platform or adjacent to it, were not affected by high grade metamorphism. The PCs in the Sava knappe, including the Sana-Una PC, close to the ensialic Tisia block, however, underwent very low and low-grade metamorphism.

The Dinaridic metallogenic province developed as a result of opening of the Vardar and Dinaridic branches of the Neo-Tethyan Ocean and its closure by convergence of the African and Eurasian plates. The northern boundary of the Dinarides is related to the northern African margin (Adria–Apulia). The Dinarides embrace well-developed and preserved tectonostratigraphic units related to the Alpine Wilson cycle, in contrast to the neighbouring Alps where the indentation of Adria obliterated or blurred their regular distribution as a result of intensive tectono-metamorphic events (Fig. 1). The major stages of the cycle are: a) Permian early intra-continental rifting, b) Triassic advanced rifting, c) Jurassic oceanization, d) Cretaceous subduction, e) Palaeogene collision; and f) Late Palaeogene/Neogene post collision and extension followed by orogenic collapse.

The metallogeny of the Dinarides, based on the principles of plate tectonics, has been upgraded over recent decades. Each stage creates characteristic ore deposits related to specific geological environments. Thermal events in the stage of early intra-continental rifting were in response to the high heat flow caused by thermal doming and thinning of the continental crust. It generated numerous hydrothermal cells in the thick piles of the postVariscan overstep successions. In addition, the incipient magmatism penetrated the Variscan basement of Pangea (PALINKAŠ et al., 2001; PALINKAŠ et al., 2010; ROTTURA et al., 1998). This stage produced numerous hydrothermal siderite-barite-polysulphide deposits, including the Ljubija ore deposits. They are the *loci typici* among the other equivalent deposits within the Dinarides, Gemerides and Eastern Alps (Fig. 1), discriminated distinctly from the deposits of the advanced rifting stage occurring in the Middle Triassic (JANKOVIĆ, 1977, 1986; PETRASCHEK, 1977; PAMIĆ & JURKOVIĆ, 1997; HEINRICH & NEUBAUER, 2002; JURKOVIĆ, 2003).

3.2. THE SANA-UNA PALAEOZOIC TERRANE

The Sana-Una PCs mostly consist of Carboniferous flysch sequences (*sensu* KARAMATA et al., 1997). The flysch is overlain by bedded limestones with conodonts of late Viséan age. A new ("post-Variscan") sedimentary cycle started with the accumulation of shallow water limestones (Stara Rijeka formation) of Bashkirian age, which rarely yield marine shallow water fossils and fusulinids. The overlying Eljdište formation (sandy and marly limestones) includes a rich brachiopod fauna. In the Una region, the Blagaj formation, covering the Carboniferous flysch, is an olistostromatic unit, termed "wild flysch" *sensu* GRUBIĆ et

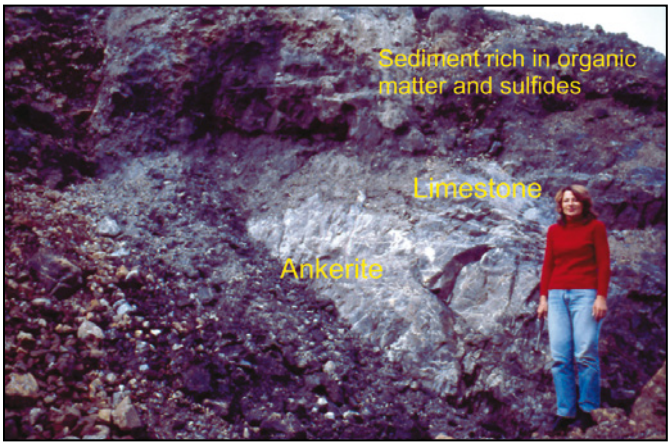

Figure 3. Dark massive siderite and ankerite in contact with dark massive limestones, the Tomašica open-cast mine.

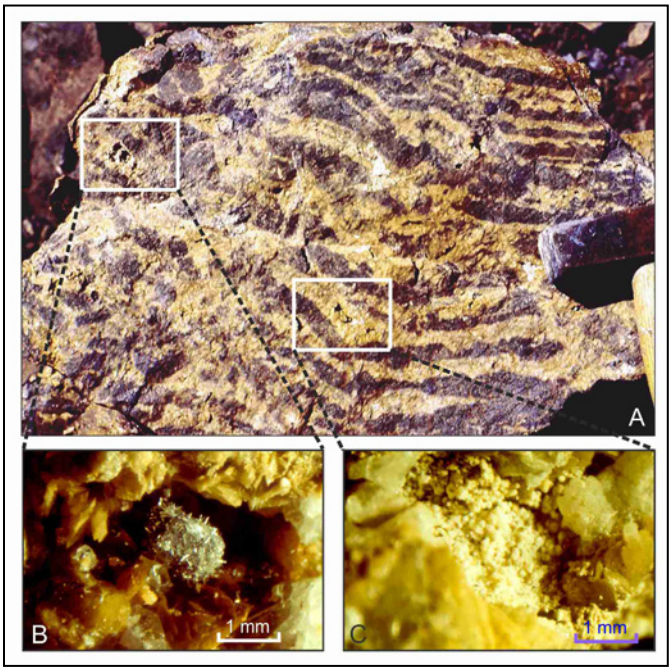

Figure 4. A) Zebra siderite comprises dark siderite and light sparry siderite bands. It contains cavities infilled with sparry ankerite, quartz, sulphides, represented mainly by galena and sphalerite (B) and alteration Li-phyllosilicates (C), Adamuša open-cast mine.

al. (2000), with Devonian, Lower and Middle Carboniferous limestone clasts containing foraminifers, corals and conodonts, and is correlated with the "molasse" type Ivovik formation from the autochthonous Jadar Block Terrain. Disconformities between the Blagaj formation and the Carboniferous flysch have not been proven. These sequences are covered by Middle Permian clastic sediments (red breccias and conglomerates, sandstones, shales and evaporites) followed by Lower Triassic formations (Fig. 2) (PROTIĆ et al., 2000; GRUBIĆ & PROTIĆ, 2003; KRSTIĆ et al., 2005).

3.3. GEOLOGY OF THE ORE DEPOSITS

The Ljubija ore deposits are placed within the Javorik flysch formation, which is well exposed within the Adamuša and the Tomašica opencast mines (GRUBIĆ et al., 2000; GRUBIĆ & CVIJIĆ, 2003). At Adamuša, the upper part of the lower flysch horizon contains irregular limestone blocks (olistostromes).

Figure 5. A) Siderite veins hosted by phyllites and metasandstones, Adamuša open-cast mine. B) Close lookup of the banded zebra texture, dark siderite, light siderite and the central white ankerite band.

Siderite with a zebra texture and sparry ankerite occur mostly within the siderite-metaclastics horizon. The Javorik flysch formation at the Tomašica opencast mine is represented by six horizons. The siderite-limonite horizon contains dark-grey massive to yellowish coarse-grained siderite and gossan composed of porous limonite. The olistostrome horizon comprises a wide variety of carbonates including dark massive limestones, dolomitic limestones, dolostones, Fe-enriched limestones, dark grey massive ankerite, and dark grey massive siderite locally weathered to porous limonite.

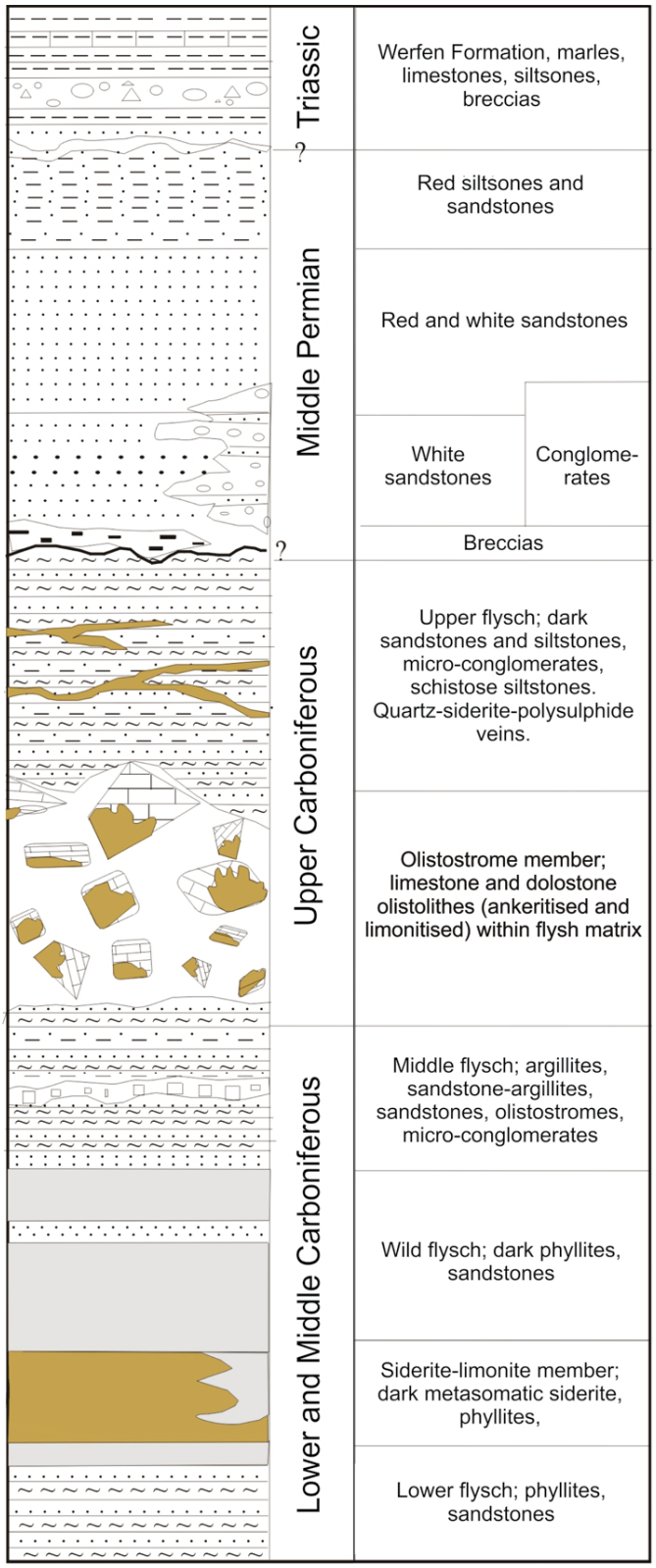

Figure 6. Stratigraphic column of the Adamuša open-cast (after GRUBIĆ et al., 2000).

3.4. ORE MINERALIZATION

The Ljubija ore field comprises the large iron ore deposits of Adamuša, Tomašica, Omarska, and Vidrenjak, and a number of smaller ones. Important reserves occur in the secondary haematite limonite ore, locally named "brand", weathering products of carbonate ores. Beside iron ores important commodities are barite and fluorite occurrences, mined in the past, scattered over the whole Palaeozoic terrain.

PALINKAŠ (1988) recognized three major types of primary iron ore textures: (1) dark massive siderite and ankerite, (2) zebra siderite composed of dark massive and light sparry siderite bands, and (3) sparry siderite veins hosted by phyllites and metasandstones (Figs. 3, 4, 5). A simplified stratigraphy for the paragenetic sequences of the Ljubija deposits is shown in (Fig. 6). Dark grey massive siderite and ankerite occur as replacements within limestone and dolostone blocks. The contacts between Fe carbonates and host carbonates are obscure. All carbonates mentioned above are dark grey in colour due to the presence of organic matter (STRMIĆ PALINKAŠ et al., 2009). A few millimetre thick white calcite veins, cross-cut dark grey limestones and are more abundant near Fe mineralisation. Similar, siderite, quartz and white calcite veins locally intersect the dark grey siderite. White sparry ankerite rarely occurs at the contact with dark massive siderite. Zebra siderite is characterized by the alternation of dark massive and light sparry siderite bands. Cavities infilled with white sparry ankerite, quartz, sulphides, and secondary phyllosilicates are common. Sparry yellowish to brownish-ochre siderite veins, thick a few decimetres, hosted by phyllites and metasandstones, represent the latest phase of mineralization.

The contact between siderite and fine-grained clastics is marked by the presence of sulphides, mainly chalcopyrite. In the eastern part of the Ljubija ore field, economically important quantities of galena, tetrahedrite, chalcopyrite, and sphalerite have been exploited in the past.

Barite and fluorite ores are present mainly as E–W oriented veins that cross-cut the Palaeozoic dolostones. The Žune-Dolinac vein type deposit was the object of this study, and was described by JEREMIĆ, 1958; (Fig. 7). A barite vein is hosted by dolostone and phyllites, close to the Scytian shales and sandstones. The vertical vein reaches 3-9 m in thickness. Barite incorporates coarse fragments of the host rocks and fluorite and quartz accumulations close to the walls. The structure and texture of the vein bears some elements of hydraulic fracturing, an important prerequisite for boiling of hydothermal fluid, as recognized in the fluid inclusion studies.

4. ANALYTICAL METHODS

4.1. MICROTHERMOMETRIC MEASUREMENTS

Microthermometric measurements were performed on double polished 0.3 to 0.5 mm thick quartz wafers and 0.05 to 0.1 mm thick fluorite wafers using a Leitz-Wetzlar microscope coupled with a Chaixmeca cooling and heating stage, operating between -180 and +600°C. Objective lenses P25/0.50 were used for

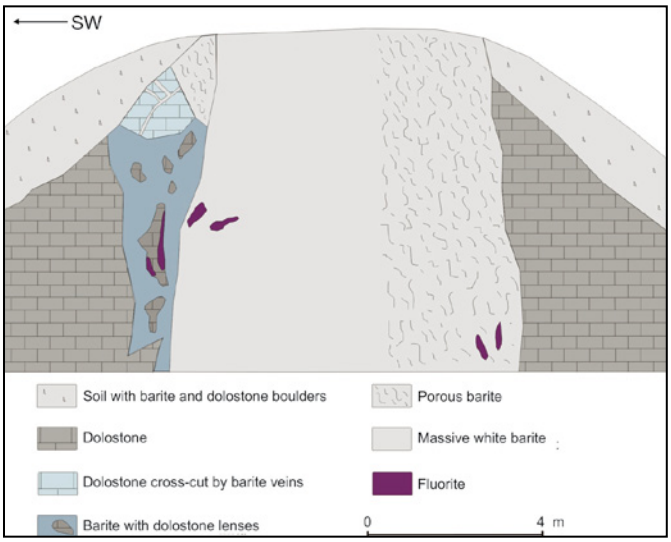

Figure 7. The cross-section of Žune-Dolinac barite-fluorite body.

freezing and UM 32/0.30 for heating runs. Microthermometric measurements on 0.1-0.2 mm thick siderite wafers were carried out using a Linkam THMS 600 freezing-heating stage mounted on an Olympus BX 51 microscope with 10x and 50x long-working distance lenses. Pure H_2O and H_2O-CO_2 synthetic fluid inclusion standards (SYN FLINC) were used to calibrate the equipment. The precision of the systems was estimated at ±2°C for heating runs, and ±0.2°C in the temperature range between -60 and +10°C. Fluid inclusions were classified according to the criteria summarised by ROEDDER (1984) and SHEPHERD et al. (1985). The salinity of aqueous inclusions was calculated by temperatures of ice and hydrohalite melting using the FLUIDS computer program for NaCl-$CaCl_2$ bearing aqueous solutions at low temperatures (BAKKER, 1999). Calculations are based on purely empirical best-fits, with no fundamental thermodynamic modelling involved (NADEN, 1996). Isochores were calculated by use of the computer program ISOC (BAKKER, 2003) using the equation of state by ZHANG & FRANTZ (1987) corrected for the volumetric properties of quartz (HOSIENI et al., 1985). The salinity of aqueous inclusions with the addition of CO_2 at the vapour phase is calculated according to COLLINS (1979).

Fluid inclusions are measured in: (i) quartz from quartz veins within dark metasomatic siderite (Adamuša locality), (ii) quartz and siderite from metasomatic zebra siderite (Adamuša locality); (iii) quartz and siderite from vein-type siderite (Adamuša locality), and (iv) fluorite from fluorite-barite vein (Žune-Dolinac locality).

4.2. IONIC CHROMATOGRAPHY, BULK CRUSH-LEACH ANALYSIS

Bulk crush-leach analyses were performed by ion chromatography at Montanuniversität Leoben. Leachates were prepared according to the technique modified after BOTTRELL et al. (1988). A Dionex DX-500 system was used for halogen analyses. Cations were measured in the aliquots of the same solution using standard atomic absorption spectrometry. Bulk fluid inclusion composition is analysed in: (i) 3 quartz, (ii) 6 siderite, (iii) a single ankerite and (iv) galena sample from metasomatic zebra siderite (Adamuša locality); (v) 3 quartz, (vi) 4 siderite, (vii) 2 barite and (viii) 2 galena samples from vein-type siderite (Adamuša locality); (ix) 2 dark host limestone; (x) a single bladed calcite (Adamuša locality); (xi) 5 fluorite and (xii) 7 barite samples from fluorite-barite vein (Žune-Dolinac locality). Equilibration temperature between ore forming fluids and the host rocks was calculated using the equation of CAN (2002), GIGGENBACH (1988), FOURNIER & TRUESDELL (1973), and VERMA & SANTOYO (1997) for geothermometric pairs Na/K, K/Mg, Na/K/Ca and Na/Li. The evaporation trend of the sea water is taken from McCAFFERY et al. (1987), and Permian and recent water from HORITA et al. (1991).

4.3. RAMAN SPECTROSCOPY

The Dilor LabRAM instrument equipped with double Nd-YAG 100 nW (532 nm) and HeNe (613 nm) lasers was used at the Institute für Geoswisssenschaften, Mountainuniversität, Leoben. The instrument is connected to an Olympus BX-40 equipped with Linkam THMSG 600 heating-freezing stage, operating between -180 and +600°C. Data were analysed using LABSPEC software. Laser Raman Spectroscopy was performed on fluorite samples from fluorite-barite vein (Žune-Dolinac locality).

4.4. VITRINITE REFLECTION

The analyses have been performed using a Leitz-MPV3 microscope-photometer, in oil, under magnification of 500× at the Organic geochemistry laboratory, INA Oil Company, Zagreb.

Samples are powdered, treated with HCl (3 days) and HF (3 days), washed and dried. Concentrated organic matter has been mixed with immersion oil and examined under the photometer. Synthetic spinel (R = 0.42 %) and garnets (R = 0.82 %; R = 1.76 %) are used for calibration. Mean random vitrinite reflectance (R_m in %) shows a strong correlation (r^2=0.7, n>600) with maximum burial temperature (T_{max} in °C). These data are modelled after BERKER & PAWLEWITZ (1994) by the linear regression equation $T = (\ln R_o + 1.68)/0.0124$, R_o = degree of vitrinite reflectance. Vitrinite reflection is determined on (i) 6 host limestone samples; (ii) host siltstones (iii) host sediment containing sulphides, and (iv) siderite samples from a metasomatic ore (all samples from Tomašica locality).

4.5. SULPHUR ISOTOPES

Sulphur isotope analyses of sulphides and sulphates selected exclusively from the primary ore samples not from the sulfides in the host rocks, were performed at the University of Lausanne using a Carlo Erba 1108 elemental analyzer (EA) connected to a Thermo Fischer Delta S IRMS (EA/IRMS). The sulphur isotope values are reported relative to a Vienna-Cañon Diablo troilite standard (V-CDT). The reproducibility, assessed by replicate analyses of laboratory standards (pyrite, synthetic mercury sulphide, working; barium sulphate), was better than ±0.2‰ (STRMIĆ PALINKAŠ et al., 2009).

4.6. GEOCHRONOLOGY

K/Ar age dating

K/Ar age dating of the whole rock samples, 21 samples of metaclastic rocks and 7 samples of volcanic rocks, are performed at the Institute of nuclear physics, Debrecen, Hungary, after the procedure described by ODIN et al. (1982).

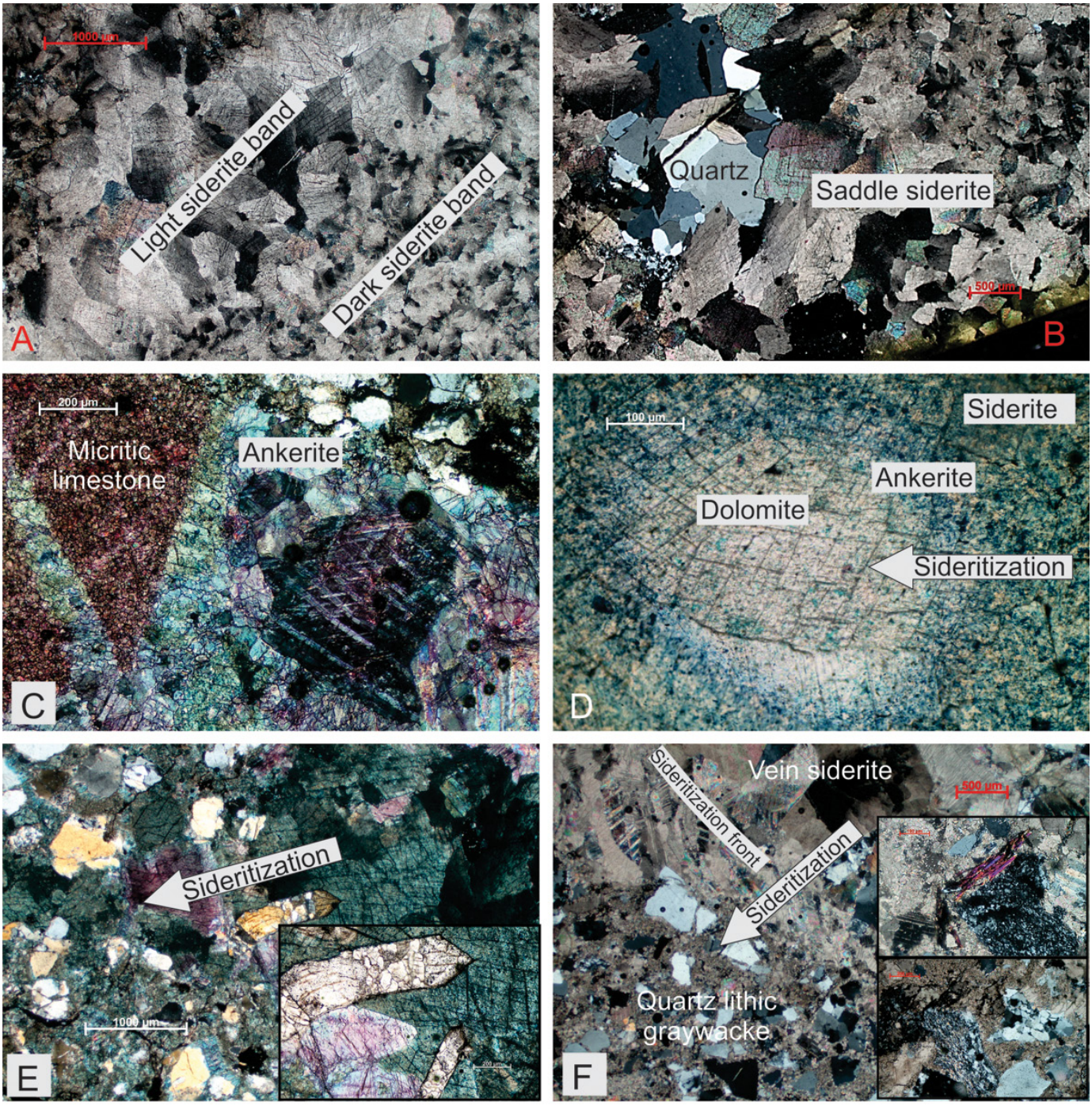

Figure 8. A) Dark and light bands in the Zebra texture (photomicrographs, crossed polars). The dark band consists of nonplanar, closely packed anhedral siderite crystals with curved, lobate and serrated boundaries. The light band is made of saddle siderite characterized by curved crystal faces or crystals with sectorial growth. The sweeping extinction indicates a warped crystal lattice. The saddle texture forms under hydrothermal conditions in the voids, between dark bands; B) The void-filling process starts with saddle siderite lining the walls and succeeded by minerals in the following order: ankerite, sulphides and quartz, not necessarily with the presence of all the successive members. The residual zones in microgeodes on the photomicrographs are lined with curved saddle siderite crystals and those with sectorial growth are filled with quartz, the object of fluid inclusion study; C) Ankerite (blue-green) replaces micritic dark limestones (pinkish red) as a sharp ferritization front (crossed polars, the colour hues come from alizarin red-S and Kferricyanide tests. Detailed description of the staining method of WARNE, 1962); D) Metasomatic replacement of late diagenetic dolomite by Fe-carbonate. The late diagenetic unimodal, planar-e dolomite, is mimically replaced by non-planar, unimodal ankerite, with curved and serrated intercrystalline boundaries. The crystal boundaries of ankerite grains gradually fade into a shapeless mass of siderite (plain-polarized light), E) Advancing sideritization front in the greywacke sandstone, with sparry siderite, develops an exotic aggregation of detrital grains. The virtual, quartz-like shape of the detrital aggregation is framed and constrained by sparry siderite crystal faces; F) An advancing sideritization front pervades greywacke sandstone forming fine grained sideritic cement. Texturally immature greywacke contains poorly sorted, angular grains of quartz and lithic fragments mostly metamorphics, slates, cherts and quarzites, set in a compact clay-fine matrix and detrital carbonaceous matter. The greywacke sandstone and black shales, a part of the „wild flysch“, originated as a product of strong turbidity currents at the edges of the continental shelves.

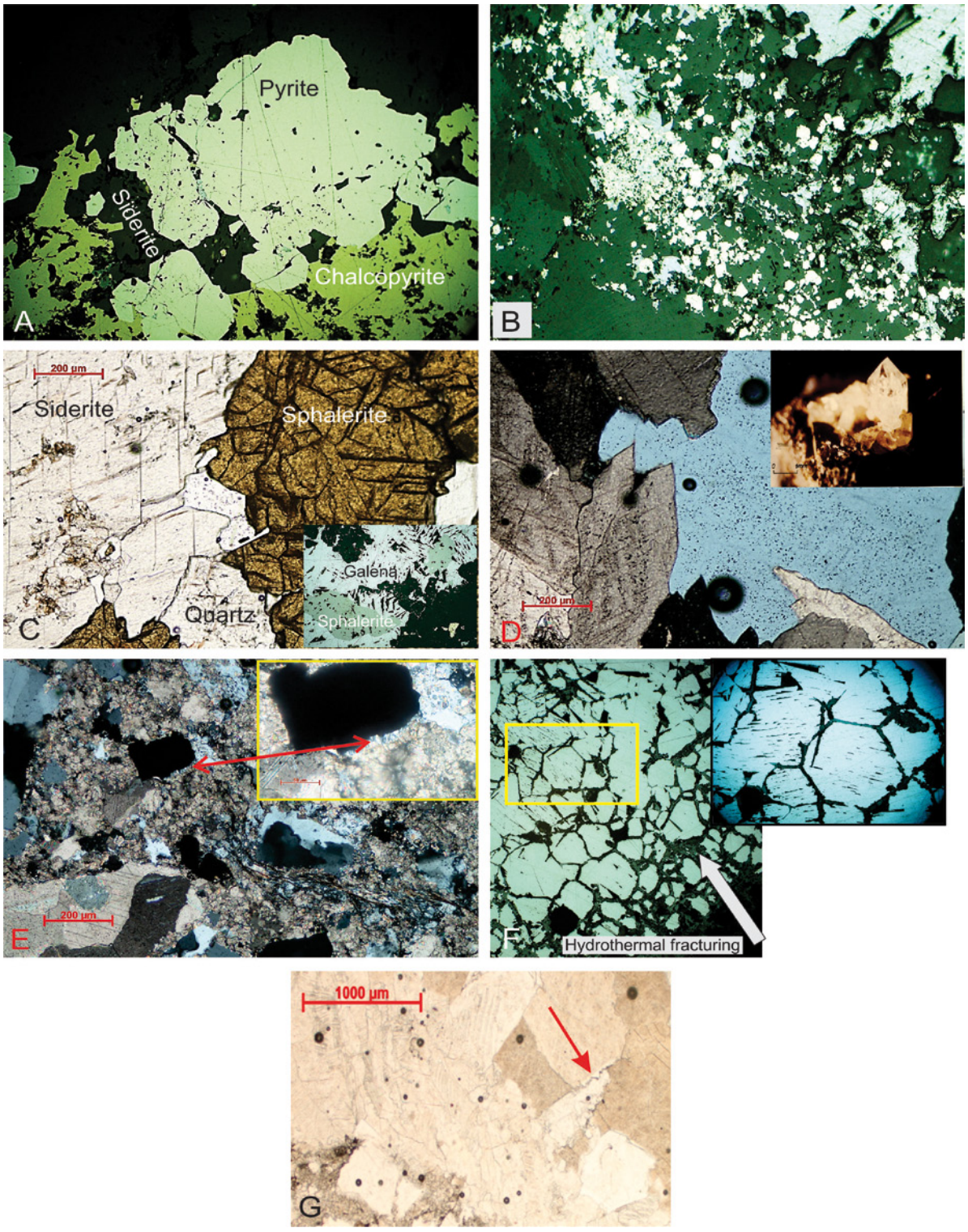

Figure 9. A) Siderite veins were formed in the late stage of mineralization in which ore bearing fluids, penetrated into the clastics, along brittle fractures and deposited sparry siderite in the open veins. While the quartz teeth grow inward from the vein walls, sulphides, pyrite, chalcopyrite and traces of galena and sphalerite fill open-spaces in the vein centre; B) Void filling processes in the light band zebra siderite proceeds with increased concentration of metasomatically released ions, Ca^{2+}, Mg^{2+}, and silica leached from incorporated clay particles in dark bands. Increased sulphur fugacity is marked by co-precipitation of finegrained pyrite and traces of galena as a veneer within sparry siderite, the major sulphide phase; C) and D) Void-filling paragenesis in the light bands of the zebra siderite; E) The host rocks underwent pervasive sideritization followed by silicification, recognized by strain fringes and strain shadows around the pyrite crystals; F) Hydraulic fracturing of galena by silica rich fluids is evidenced by jig-saw-fit texture with fragments stuck together by silica cement. Absence of grain boundary migration and rotation, evidenced by near parallel cleavage among the galena grains, which already past static recrystallization (triplet junction), is a sign of low temperature recrystallization in the following mineralization history; G) Penetrative fabrics might have been developed by crystallization pressure in veins, evidenced by stylolites between sparry siderite grains, or as low grade metamorphism in the presence of water when pressure solution was dominant (MERINO et al., 2006).

^{40}Ar/^{39}Ar analyses

^{40}Ar/^{39}Ar analyses were carried out at the ARGONAUT Laboratory of the Division of General Geology and Geodynamics at the University of Salzburg. A single white mica concentrate from vein-type siderite was irradiated in the MTAKFKI reactor (Debrecen, Hungary). ^{40}Ar/^{39}Ar analysis was carried out using a UHV Ar-extraction line equipped with a combined MERCHANTEK-TM UV/IR laser ablation facility and a VG-ISOTECHTM NG3600 Mass Spectrometer. Isotopic ratios, ages and errors for individual steps are calculated following suggestions by MC-DOUGALL & HARRISON (1999) and using decay factors reported by STEIGER & JÄGER (1977). Definition and calculation of plateau ages was carried out using ISOPLOT/EX softwer (LUDWIG, 2001, 2005).

5. RESULTS

5.1. PETROGRAPHY

Transmitted and reflected light microscopy supports the genetic interpretation of the ore textures (Figs. 8, 9). The three major type of textures are (i) dark grey massive siderite, (ii) zebra texture with dark and light siderite bands, and (iii) vein siderite.

(i) Dark massive siderite was formed by volume-per-volume replacement of dolostones and limestones by Fe-saturated solution (Fig. 3). Metasomatizm is recongnized by the unimodal size of siderite grains, with nonplanar boundaries, non-mimical replacement of dolomite allochems, and traces of indigenous organic matter which still gives a dark colour to the bands. The nonplanar boundaries are characteristic of growth at elevated temperature and/or high supersaturation, as neomorphism of a precursor dolostone or limestone (Fig. 8D) (SIBLEY & GREGG, 1987).

(ii) Formation of the zebra texture is a combination of two different processes, replacement as simultaneous solution and deposition of siderite, in the manner of atom-per-atom, expressed by reactions 1) and 2).

1) $CaCO_3 + Fe^{2+} = FeCO_3 + Ca^{2+}$

$\Delta V_{reac} = -22\%$, $\Delta G_{reac\ 500} = -27.95$ kJ

$\log K_{reac\ 500} = 2.91$, T = 500 K

$\Delta \bar{G}_{reac\ 500} = -27.95 + 9.59 \log a_{Ca^{2+}} - 9.59 \log a_{Fe^{2+}}$

2) $(Ca,Mg)CO_3 + 2Fe^{2+} = 2\ FeCO_3 + Ca^{2+} + Mg^{2+}$

$\Delta V_{reac} = -11\%$, $\Delta Gr_{reac\ 500} = -43.7$ kJ

$\log K_{reac\ 500} = 4.5$, T = 500 K

$\Delta \bar{G}_{reac\ 500} = -43.7 + 9.59 (\log a_{Ca^{2+}} + \log a_{Mg^{2+}}) - 19.18 \log a_{Fe^{2+}}$

It is accompanied by a significant change of volume, $\Delta V_{reac\ \%} = -22\%$ and -11%. A difference between the molar volume of siderite and precursor limestone/dolomite, leaves open space for sparry siderite in the zebra texture. Replacement is sustained by infiltration of an iron rich hydrothermal fluid, rather than by restricted diffusion *sensu* KORZHINSKII (1968).

The succeeding step was the crystallization of saddle style siderite in open voids from Fe-impoverished and Ca^{2+}/Mg^{2+}-enriched fluids. This highly variable concentration and composition of the fluid is a cause for the growth of curved crystal faces and sweeping extinction of saddle siderite (Fig. 4A, 8B; 9D) (SAERL, 1989):

3) $Fe^{2+} + CO_3^{=} = FeCO_3$

$\Delta G_{reac\ 500} = -12.26$ kJ

$\log K_{reac\ 500} = 1.27$, T = 500 K

$\Delta \bar{G}_{reac\ 500} = -12.26 - 9.59 \log a_{Fe^{2+}} - 9.59 \log a_{CO_3^{=}}$

This is a typical of open space filling processes identified by many vugs and cavities, coarsening of minerals from the walls of the voids to their centre, comb structure or interdigitated vuggy zone, and symmetrical banding. The void-filling process starts with saddle siderite, lining the walls and proceeds in the following sequential mineral order: ankerite, quartz and sulphides, not necessarily with the presence of all the successive members (Fig. 9B, 9D).

Some thermodynamic consideration of the free energy change ($\Delta \bar{G}_{reac}$ 500) at 500 K (227°C) confirms the preference of reactions (1) and (2) during the early metasomatic phase, and the formation of dark bands. The increase of Ca^{2+}/Mg^{2+} concentration increases $\Delta \bar{G}_{reac}$ 500 and supports the tendency of reaction (3) to dominate during crystallization of light sparry siderite bands. The presence of CO_2 (recognized at the trace level by Raman spectroscopy) is an irrelevant variable in the reactions (1) and (2) and equilibria is controlled by the $Fe^{2+}/Ca^{2+}Mg^{2+}$ratio. Reaction (3) proceeds under neutral and slightly alkaline conditions, buffered by carbonate host rocks and the dominant species are HCO_3^- and $CO_3^{=}$, and fugacity of CO_2 is negligible. It is not the case in the siliciclastic host rocks, during development of barite vein deposits, whereas liquid CO_2 also participated in the control of pressure and boiling (BOROJEVIĆ ŠOŠTARIĆ et al., 2009).

(iii) Siderite veins, another structural facet of the ores, were formed by mineralizing fluids, enriched in Fe-bicarbonate ions by widespread collateral metasomatic reactions (Fig.5). They penetrated into the shales, silts and sandstones, along planar discontinuities caused by fault slip events under brittle conditions and deposited sparry siderite in open veins with fuzzy boundaries (Fig. 9E). The host rocks underwent pervasive sideritization during the mineralization phase followed by silicification, recognized by antitaxial strain fringes and strain shadows around the rigid pyrite porphyroblasts. Characteristic dilatation sites were formed by silica rich fluids at low-temperature (200-300°C) and high fluid pressure (OLIVER & BONS, 2001). Enrichment of the silica component in the fluids came from the alteration of phyllosilicates and residual clay particles in the carbonate precursor. The best conduits of the fluids were dark seams, composed of organic detritus, phyllosilicates, and insoluble material, deformed around a rigid object, e.g. a corroded detrital quartz grain (Fig. 9E). Hydraulic fracturing of galena is another aspect of the high fluid pressure (Fig. 9F). The galena triple-junction system, forms a hexagonal network of recrystallized grains, which underwent fracturing, sustaining a jig-saw-fit texture with fragments stuck together with silica cement (lower corner of Fig. 9F).

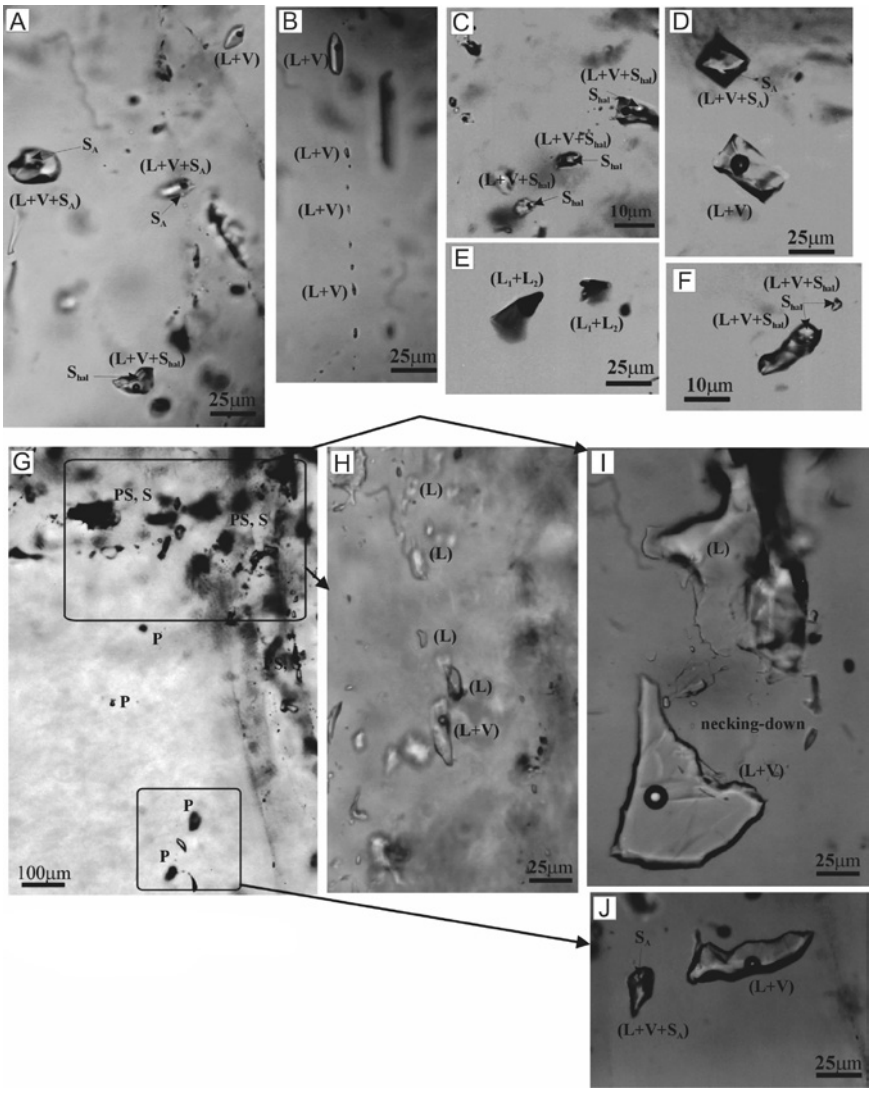

Figure 10. Fluid inclusions in quartz from void-fillings in the zebra siderite, and mesothermal siderite-quartz veins in the greywacke (Ljubija/Adamuša). a) „Zebra siderite": primary (L+V+Shal), (L+V+SA) and (L+V) inclusions, Type I and II; b) Array of primary inclusions (L+V), Type II with the same degree of filling; c) Array of primary (L+V+Shal) inclusions; d) Primary (L+V) and (L+V+SA) inclusions, Type II; e) Primary inclusions with immiscible fluids (L1+L2), Type III; f) Primary inclusions (L+V+Shal), Type I. Mesothermal siderite-quartz veins: g) Quartz with marked primary (P), pseudosecondary (PS) and secondary (S) inclusions; h) Array of liquid inclusions, Type IV; j) Primary (L+V) and (L+V+SA) inclusions, Type III (see text).

The quartz grain shows clear signs of dynamic recrystallization by development of subgrains and gradual bulging (STIPP et al., 2002). Beside fluid inclusion data, deformation lamellae in siderite crystals could be used as an approximate temperature gauge of vein formation. Narrow straight twins (Fig. 9E, type I, BURKHARD, 1993) indicate temperatures bellow 170°C. The tabular thick twins, which can be optically resolved (Fig. 8C, type II, >1µm, FERRIL et al., 2004), dominate above 200 °C and up to 300°C. Penetrative fabrics which might be related to the crystallization pressure in veins, are evident by stylolites between sparry siderite grains (Fig. 9G, MERINO et al., 2006). The siderite walls of the vein include quartz-comb textures grown inward, accompanied by pyrite, chalcopyrite, traces of galena and sphalerite (Fig. 9A). Chert and schist fragments in the greywacke are inherited porphyroclasts from the Variscan high-grade metamorphic provenance, incorporated during the turbidite phase (Fig. 8F).

5.2. FLUID INCLUSION STUDY

Fluid inclusion studies in quartz from quartz veins within the dark metasomatic siderite (Adamuša locality)

Quartz veins are several mm to 10 cm thick containing milky white quartz. At several places open space cavities are found containing half-transparent idiomorphic quartz, several millimetres in size. Fluid inclusion petrography shows the presence of primary and pseudosecondary liquid-rich inclusions of a uniform degree of fill. Eutectic melting occurs at temperature ranges from -39.4 to -21.0ºC. Ice melting in the temperature range from -23.9 to 1.5ºC shows salinities from 23.4 to 2.1 wt.% NaCl equiv. Homogenization by vapour disappearance occurs in a temperature range from 80 to 160ºC.

Fluid inclusion study in quartz from cavities within metasomatic zebra siderite (Adamuša locality)

The investigated quartz follows precipitation of light zebra siderite, and precedes the precipitation of sulphides (galena, sphalerite, chalcopyrite, pyrite) within the cavities. Quartz crystals are idiomorphic, transparent up to 1 cm in size. They contain numerous fluid inclusions which are located within growth zones and classified as primary according to the criteria outlined by ROEDDER (1982): Type I; Liquid-rich four phase, aqueous inclusions containing a halite daughter mineral, also sometimes contain an unknown anisotropic daughter mineral, ($L+V+S_{hal}\pm S_A$); Type II; Liquid-rich three phase aqueous inclusions, containing an unknown anisotropic daughter mineral ($L+V\pm S_A$), high salinity; Type III; Inclusions contain immiscible liquids (L_1+L_2). Type IV; Monophase liquid

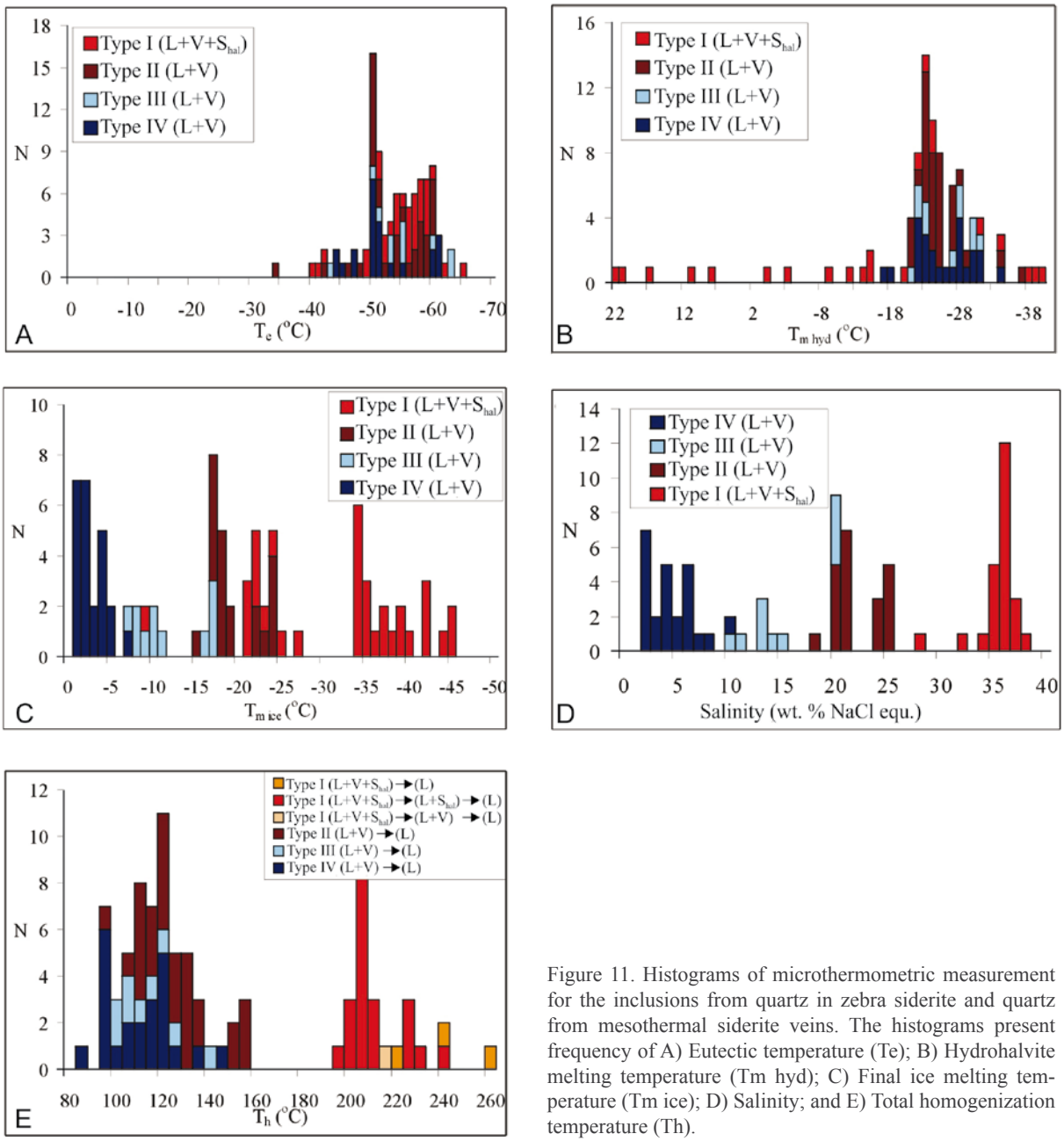

Figure 11. Histograms of microthermometric measurement for the inclusions from quartz in zebra siderite and quartz from mesothermal siderite veins. The histograms present frequency of A) Eutectic temperature (Te); B) Hydrohalvite melting temperature (Tm hyd); C) Final ice melting temperature (Tm ice); D) Salinity; and E) Total homogenization temperature (Th).

inclusions, liquid inclusions containing a halite daughter mineral (L±V±S_{hal}) and (V); Monophase gas inclusions (Fig. 10). The study was focused on a primary assemblage of aqueous inclusions. Within halite bearing inclusions eutectic melting occurs in a temperature range from -65.7º to -51.0ºC, followed by ice melting in the temperature range from -44.2º to -21.6ºC, and hydrohalite melting (transformation to halite) at a temperature range of -40.9º to +0.1 ºC. Under metastable conditions, hydrohalite exists up to 22ºC in a few inclusions. In addition, several inclusions show melting of an unknown, optically isotropic phase at a temperature range from -35.0º to 36.1ºC. Total homogenization occurs in the temperature range from 201ºC to 259 ºC, showing salinities from 35 to 39 wt.% NaCl equiv. During homogenization, inclusions show different behaviours: (i) the disappearance of vapour follows the disappearance of halite; (ii) the disappearance of halite follows the disappearance of vapour, or (iii) halite and vapour disappear simultaneously.

The case of simultaneous disappearance of vapour and halite occurs at temperature ranging from 220º to 259ºC. The existence of three and the disappearance of two phases (L+V+S_{hal}→L) in the NaCl-H_2O system (T_h total), is univariant equilibria which enables determination of fluid pressure and salinity (32.9-35.3 wt.% NaCl equiv.). Thermochemical properties of the H_2O-NaCl saturated solutions (HAAS, 1976) constrain the pressure at 16.5 bars or 32.7 bars, respectively. Halite undersaturated inclusions show eutectic melting at temperatures ranging from -60º to 51ºC, followed by hydrohalite melting at temperatures ranging from -27.5º to -20.8ºC. Ice melting in a range from -23º (undercooling below 21.2 ºC) to -2.5ºC, indicate salinities from 22.5 to 3.5 wt. % NaCl equiv. They all homogenized by vapour disappearance, in the temperature range of 11º - 210ºC.

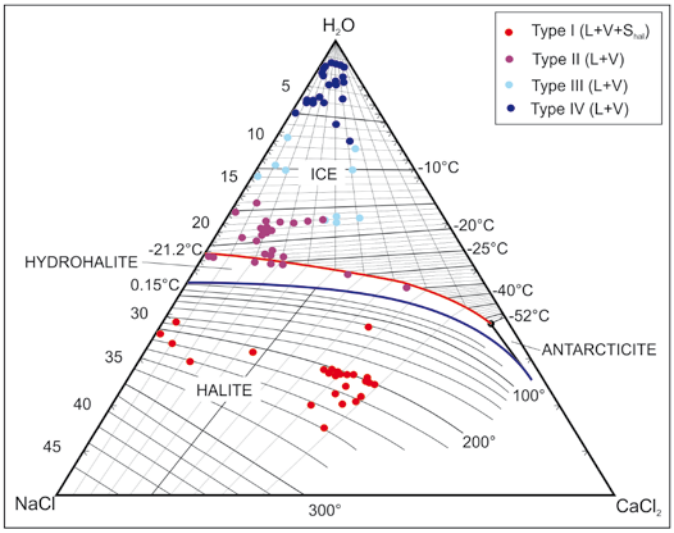

Figure 12. Ternary-component diagram NaCl-$CaCl_2$-H_2O for all measured inclusions in Ljubija/Adamuša ore field. Shift of composition from NaCl-H_2O line toward $CaCl_2$-H_2O line is a result of metasomatism. A wide variation of salinity points to the mixing of two contrasting fluids, high density FLUID 1with low density FLUID 2.

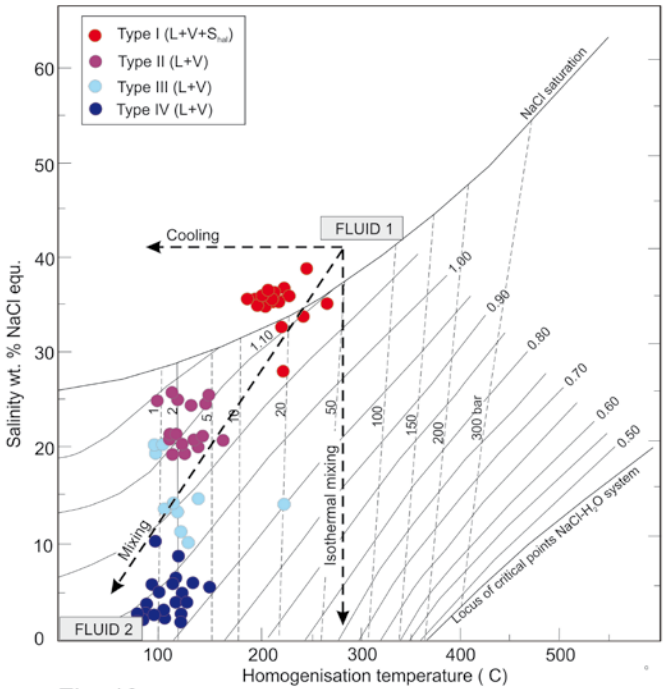

Figure 13. Diagram of temperature of homogenization vs. salinity, Ljubija/Adamuša for fluid inclusions in the ore field Ljubija/Adamuša, another confirmation of the mixing of two contrasting fluids, high salinity, high temperature FLUID 1 and low salinity, low temperature FLUID 2.

The extremely low eutectic temperature (T_e) observed in some quartz samples could be interpreted as a metastable eutecticum in $CaCl_2$-NaCl-H_2O or $MgCl_2$-NaCl-H_2O systems (DAVIES et al. 1990), but can also be explained by the presence of Li^+ ions in ore bearing fluids as well.

Fluid inclusion study in siderite from metasomatic zebra siderite (Adamuša locality)

Fluid inclusions have been studied in siderite crystals separated from light bands within metasomatic zebra ore. Most inclusions in siderite crystals are two-phase (L+V) and can be defined as primary. They acquire negative crystal, or irregular, three-dimensional shapes and are distributed irregularly within the crystals. Primary inclusions show consistent liquid–vapour (L/V) volume ratios, which indicate entrapment of a homogenous fluid. The eutectic temperature spans the range between -53° and -49.9°C, suggesting a $CaCl_2$-NaCl-H_2O system. Hydrohalite melting occurs in the narrow range between -31.1° and -29.0°C. Ice melting temperatures recorded in an interval from -12.0° to -10.1°C corresponds to a salinity between 14.1 and 16.0 wt.% NaCl equiv. Total homogenization, always into the liquid phase, ranges between 147 and 164°C. Secondary two-phase (L-V) inclusions are recorded as well, but they have not been measured due to their small size.

Fluid inclusion study in quartz from hydrothermal quartz-siderite veins (Adamuša locality)

Vein-type siderite contains two types of quartz crystals: irregular, milky white quartz which does not contain measurable FIs, and semi-transparent quartz-siderite intergrowth, containing Type III; Primary liquid-rich inclusions, with or without an anisotropic daughter mineral, (L+V±S_A); Type IV; Pseudosecondary liquid-rich inclusions (sometimes with an anisotropic daughter mineral), (L±V±S_{hal}) generating vapour bubbles after the freezing run. This is either a sign that our fluid inclusions were stretched during the freezing run or just metastability is affecting the re-apperance of the vapour phase after freezing.

Primary inclusions show eutectic melting at temperatures ranging from -63ºC to -43ºC, followed by hydrohalite melting at temperatures from -31.0º to -21ºC. Salinities calculated from the ice melting temperatures (-17.7º to -7.1ºC) ranged from 20 to 11.5 wt.% (in those inclusions with the presence of a vapour phase at room temperature) NaCl equiv. Several inclusions show eutectic melting at -4.7ºC and gas hydrate melting at +10ºC, suggesting the presence of bicarbonates and CO_2 hydrates. Homogenization was in the range from 97º to 250ºC. Pseudosecondary liquid-rich inclusions show eutectic melting at temperatures between -60º to -44ºC, followed by hydrohalite melting between -34º to 22ºC and ice melting between -7.1º to -1.4ºC. Calculated salinities ranged from 2.0 to 9.0 wt.% NaCl equiv., whereas homogenization temperatures (by vapour disappearance) range from 90º to 133ºC.

Fluid inclusion study in siderite from hydrothermal quartz-siderite veins (Adamuša locality)

Several primary fluid inclusions have been recorded in sparry siderite crystals from siderite veins hosted by the Carboniferous shale. A eutectic temperature around -52°C suggests a $CaCl_2$NaCl-H_2O system. Hydrohalite melting spans an interval between -29.5° and -21.0°C. Ice melting temperature recorded between -4.2° and -3.5°C points to a salinity between 5.7 and 6.7 wt.% NaCl equiv. Homogenization into the liquid phase occurs in the range from 120° to 127°C.

Results of microthermometric measurements on quartz from the three principal types of the Fe mineralisation in Ljubija/Adamuša are presented in Fig. 11.

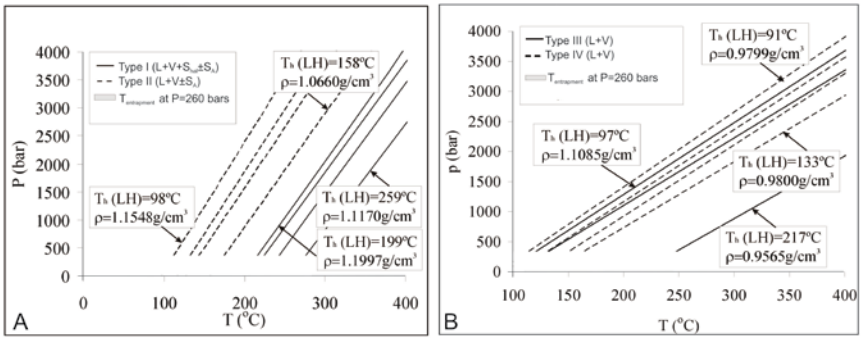

Figure 14. A) Isochores for the end members (L+V+Shal±SA) inclusions Type I, and (L+V±SA) Type II in the quartz from zebra siderite, and B) end members inclusions (L+V±SA) Type III and IV in quartz from the mesothermal siderite veins.

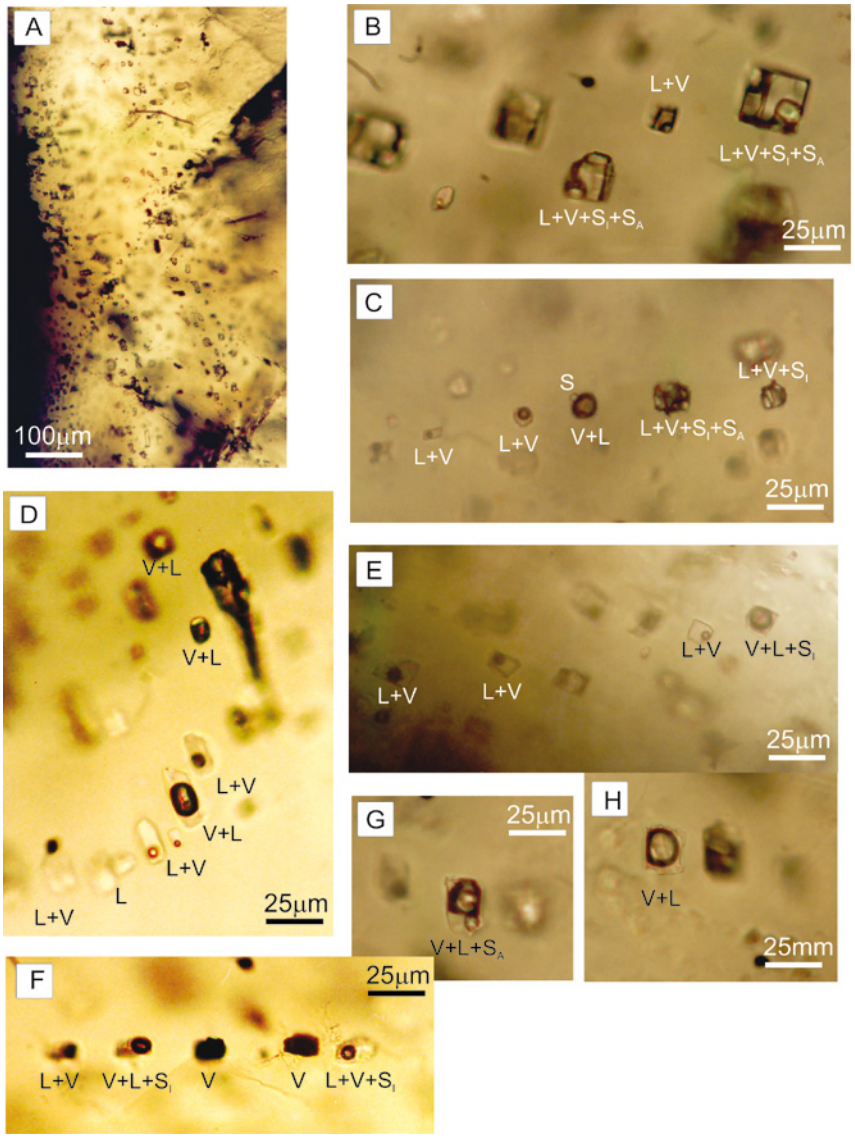

Figure 15. Fluid inclusions in fluorite in the barite-fluorite vein ore body Žune-Dolinac; A) Array of primary inclusions in the central part of the fluorite crystal; B) Primary FI-s (L+V+Shal+SA), Type I and (L+V) Type III; C) Boiling effects – array of Fis with different degrees of filling (L+V), (V+L), (L+V+Shal+SA) and (L+V+SA), Type II, III, IV, V; D) Boiling effect – array of primary FIs (L), (L+V), (V+L), Type III, IV and IX; E) coexistance of (L+V) and (L+V+Shal) Fis Type I and II; F) Boiling effects – array of primary (L+V), (L+V+Shal), (V), Fis Type I, II and VII; G) Primary (L+V+SA) FI Type II; and H) Primary (V+L) FI Type IV. Important note, the listed types of fluid inclusions coexists within one single grain. Graphical presentation of fluid inclusions depicting the great variability in salinity, density, number of phases, different solids, indicate a boiling system, and are presented in the drawing Fig. 16.

A ternary diagram NaCl-$CaCl_2$-H_2O (Fig. 12) for all types of FIs in the Ljubija/Adamuša deposit shows a shift of data points from the NaCl-H_2O line toward the $CaCl_2$-H_2O according to the dominant metasomatic process. The diagram also emphasizes the wide distribution of salinity from very low to very high. An explanation is suggested by the diagram T_h vs. salinity (Fig. 13). The diagram shows a wide range of high to low salinity, and a narrow but declining trend of T_h, from high to low, which suggests the mixing of the two types of contrasting fluids. The high temperature, high salinity, Type I, true evaporitic brine, and the low temperature, low salinity Type II, indicating that the sea water not only evolved by evaporation. Mixing happened a few hundred metres close to the topographic surface. A P-T diagram with isochores calculated by the ISOC computer program is presented in Figure 14.

Fluid inclusion study in fluorite from a fluorite-barite vein (Žune-Dolinac locality)

Purple fluorite crystals with well developed growth zones were selected for the fluid inclusion analysis. The petrography revealed the presence of various inclusion types, classified as primary: type I; Liquid-rich aqueous inclusions containing a halite daughter mineral and an unknown anisotropic daughter mineral, high salinity ($L+V+S_{hal\pm}S_A$) (Fig. 15B), Type II; Liquid-rich aqueous inclusions containing an anisotropic daughter mineral, high salinity ($L+V\pm S_A$), (Fig. 15B), Type III; Liquid-rich aqueous inclusions (L+V), low to moderate salinity, (Fig.15D), Type IV; Vapour rich aqueous inclusion ($V+L\pm S_A$), low to moderate salinity, possibility of leaking (Fig. 15), Type V; Vapour rich with halite daughter mineral ($V\pm L+S_{hal}$) (Figs. 15E,F), Type VI; Two immiscible liquids (L_1+L_2), no sign of fluorescence, neither freezing, Type VII; Vapour inclusions (V) (Fig. 15F), Type VIII; Solid inclusions (S_A) (Fig. 15C), anisotropic mineral present in the Types I, II, and IV. Type IX; Liquid inclusions (L), (Fig. 15D), (important note that all numbered types coexist within one single grain, Fig. 16).

Fluid inclusion study was performed on liquid rich and vapour rich inclusions with or without daughter minerals. Halite saturated aqueous inclusions (± unknown anisotropic daughter mineral) Type I and II show first melting at temperatures from -66.4º to 49.0ºC, followed by ice melting in the tem-

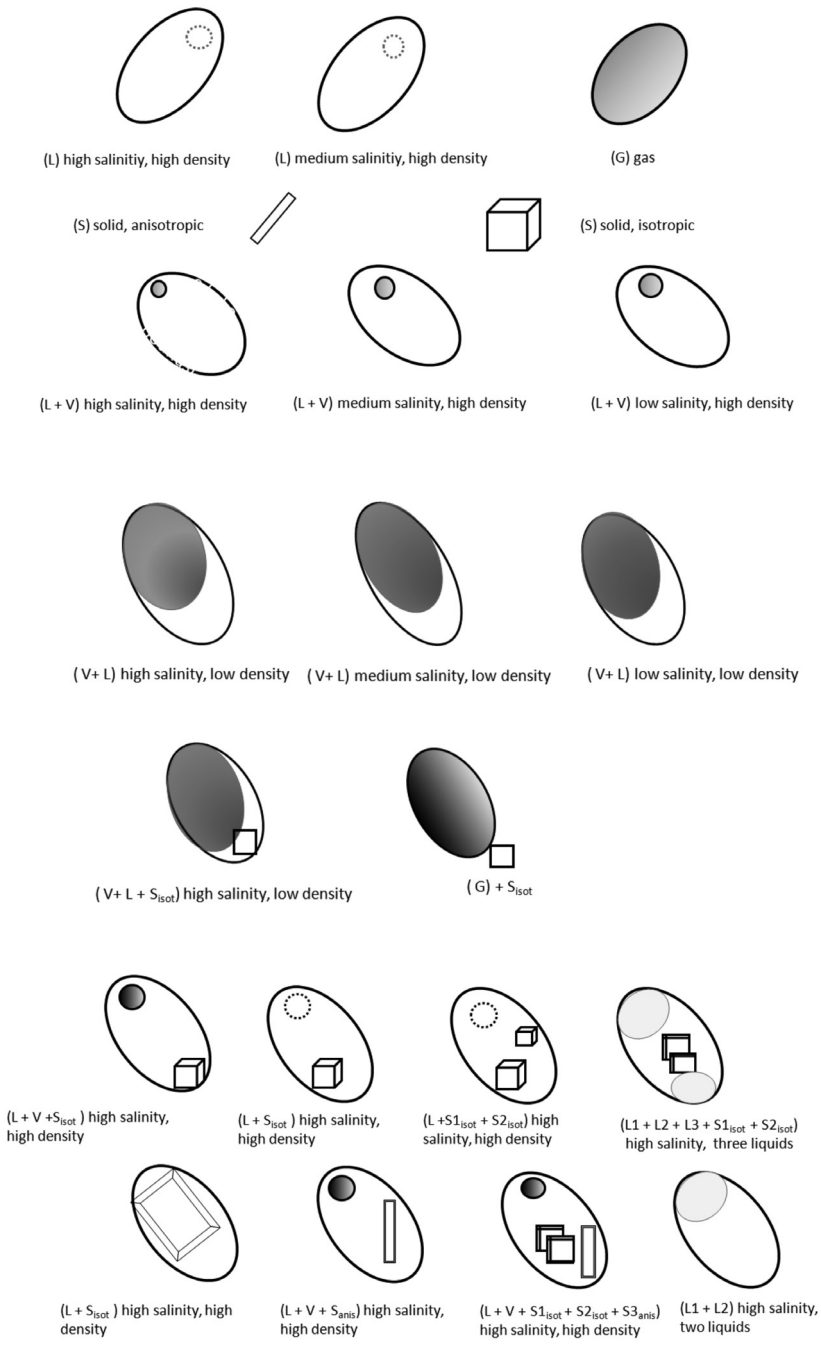

Figure 16. Selection of fluid inclusion types in one single crystal of fluorite, Žune-Dolinac locality (PALINKAŠ, 1988).

perature range from -41.2 to -21.6ºC and hydrohalite melting/transformation between -35.5º to -1.2ºC. During heating, within the majority of the inclusions, the vapour phase disappeared first, followed by halite dissolution in the temperature range between 125º - 297ºC. A single inclusion melted sylvite at 129ºC followed by halite melting at 139ºC. Several inclusions melted halite in the temperature range from 8.1 to 11.4ºC, followed by the disappearance of the vapour phase at temperatures between 145 - 238ºC. Salinities are between 26.0 and 41.7 wt% NaCl equiv. Halite undersaturated aqueous inclusions (L+V), Type III; show similar eutectic temperatures (T_e = -65.0º to -49.0 ºC), followed by hydrohalite melting (T_{hyd} = -35.6º to -21.0ºC). Salinities are calculated from ice melting temperatures (T_{ice} = -21.1 to -1.2 ºC) and range from 25 to 3.5 wt% NaCl equiv. Homogenization into a liquid phase was in a temperature range from 175 to 275ºC. Type IV, vapour rich aqueous inclusions show eutectic melting in a temperature range from -56º to - 48ºC, followed by hydrohalite melting (T_{hyd} = -44º to -21ºC) or ice melting (T_{ice} = -38º to -3.1ºC). Salinities range from 33.4 to 5.1 wt% NaCl equiv, whereas homogenization to a vapour phase occurred in the range from 125º to 245ºC. Several inclusions decrepitated during heating procedure (Fig. 17).

The co-existence of liquid rich inclusions Type II, (L+V+S_{hal}), of high salinity from 25 to 42 wt% NaCl equiv, and Type IV, vapour rich (V+L) with very low salinity between 0.4 to 5 wt% NaCl equiv, homogenizing in the same temperature interval between 125 and 245 ºC, corroborate the indication of boiling.

The inclusions with halite as the last homogenization phase after (L+V+S_{hal})→(L+S_{hal}) →(L) at 300ºC, and vapour rich inclusions with halite crystals (V+S_{hal}), and those with solid halite inclusions (S_{hal}) are the product of a distillation (boiling evaporation) process in a semiclosed system with variable pressure, communicating with the open space on the earth surface followed by heterogeneous trapping. However, the behaviour of these high salinity and low salinity FI-s, especially the type (V+S_{hal}), and solid inclusion (S_{hal}) cannot be explained by one single episode of boiling. This impressive collection of fluid inclusion types, (more than 9 in one single crystal) requires multistage episodes of boiling producing a mixture of liquid water and bubbles, suspension of crystalls, halite, sylvite, and unknown solids, trapped into one single crystal. It represents repeated boiling episodes under changable pressure, due to a change in hydraulic head, water table, pressure of gases (suspected hydrocarbon liquids in inclusions), breakage of sealing, or maybe the intrusion of hot superheated water or steam from below into low salinity meteoric water, causing the rise of vapour and boiling, etc. The ternary diagram NaCl-$CaCl_2$-H_2O (Fig. 18), also indicates the boiling process. The T_h vs. salinity diagram also confirms boiling and the separation of high salinity liquids from low salinity vapour (Fig. 19). In this plethora of FI-s types and disequilibrium conditions, there was an attempt to determine the pressure of boiling by coexisting inclusions in one crystal, 33.4 wt% NaCl equiv. (L+V), and 0.4 wt% NaCl equiv. (V+L), and homogenization at the same temperature, (Th), at 245ºC which yields 36.1 bars. Applying hydrostatic pressure, the depth of boiling would be 361 m (HAAS, 1976, 1971).

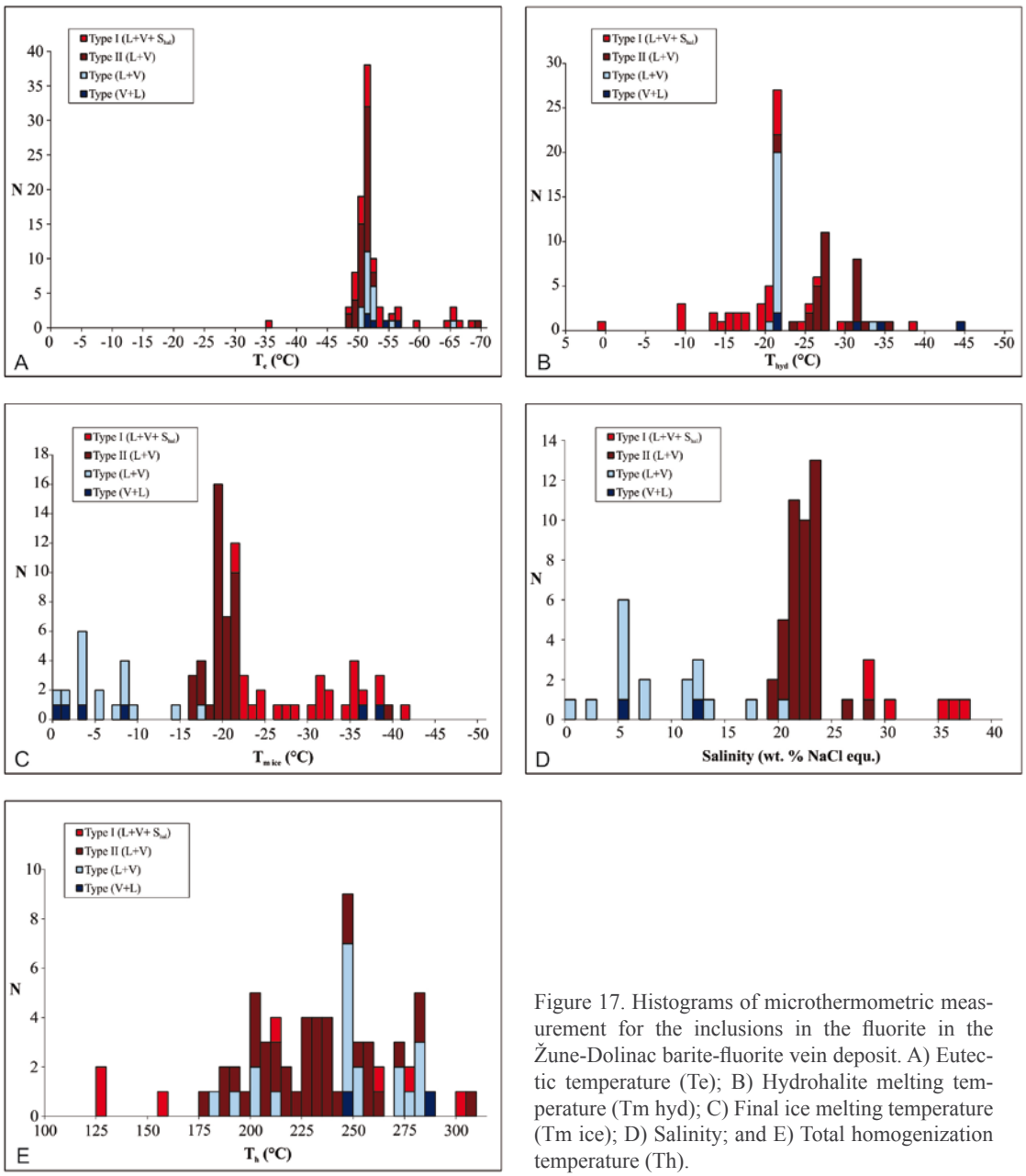

Figure 17. Histograms of microthermometric measurement for the inclusions in the fluorite in the Žune-Dolinac barite-fluorite vein deposit. A) Eutectic temperature (Te); B) Hydrohalite melting temperature (Tm hyd); C) Final ice melting temperature (Tm ice); D) Salinity; and E) Total homogenization temperature (Th).

5.3. LASER RAMAN SPECTROSCOPY

Laser Raman spectroscopy was performed on fluid inclusions from fluorite (fluorite-barite vein, Žune-Dolinac locality) on the four-phase, (L+V+$S_{hal\pm}S_A$) Type I; the three-phase, (L+V±S_A) Type II; two-phase (L+V) Type III. Liquid-rich aqueous inclusions containing halite daughter minerals, with high salinity. At room temperature they are composed of aqueous liquid (broad shoulder at around 3400 cm^{-1}) and aqueous gas and/or traces of CO_2 (peaks at 1278 and 1383 cm^{-1}). Other volatiles were not detected. At -21ºC fluid inclusions contain ice (a broad peak at 3100 cm^{-1}) and hydrohalite (a doublet around 3418 cm^{-1} and a sharp peak at 3543 cm^{-1}).

5.4. BULK CRUSH-LEACH ANALYSES

Bulk crush-leach analysis by ionic chromatography was performed on quartz, siderite, ankerite and galena from metasomatic zebra-type siderite; quartz, siderite, barite and galena samples from vein-type siderite, dark host limestone; bladed calcite (Adamuša locality) and fluorite and barite samples from a fluorite-barite vein (Žune-Dolinac locality, Table 1).

Recalculated bromine contents from leachates in quartz from metasomatic zebra siderite are elevated and vary between 535 and 685 ppm, whereas within vein-type siderite varies between 165 and 256 ppm (according to the procedure outlined by CHANNER et al. (1999). The recalculated bromine concentration in fluorite from the Žune-Dolinac locality is similar to the quartz from the metasomatic zebra-type siderite, ranging from 430 ppm to 605 ppm. A high concentration of bromide is registered in the dark limestone and barite as well.

Na^+, Ca^{2+}, K^+, and $Mg^{2+}$are major cations, while the dominant anion is Cl^- followed by SO_4^{2-}. These data correspond to the observed low eutectic temperature and depression of hydrohalite melting, both indicating the presence of divalent cations within the fluids, with the exception of Mg^{2+} which is

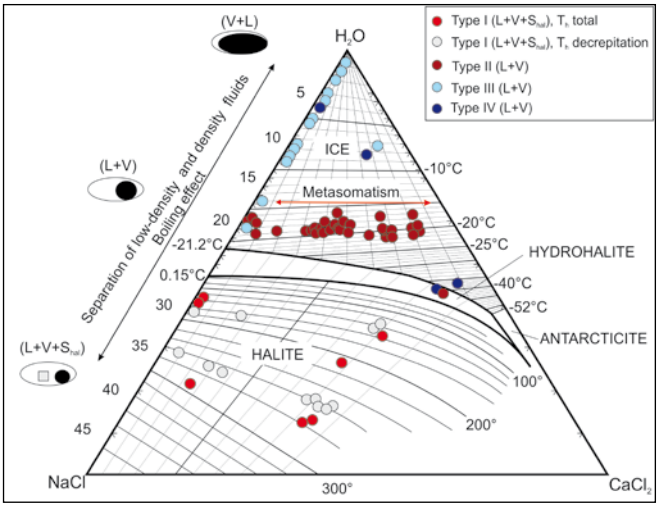

Figure 18. Ternary-component diagram NaCl-$CaCl_2$-H_2O for all types of inclusions in fluorite from the Žune-Dolinac barite-fluorite vein deposit, Ljubija ore field. Shift of composition from NaCl-H_2O line toward $CaCl_2$-H_2O line is a result of metasomatism. Differentiation of high salinity and low salinity inclusions, however, could be attributed to the extensive boiling processes determined in the deposit.

below the detection limit within quartz zebra siderite. It explains the precipitation of ankerite in the middle of the light bands, and the formation of saddle siderite crystals. High Ca^{2+} and Mg^{2+} concentrations are the direct results of intensive metasomatic ankeritization and sideritization.

Concentration of sulphate is between 0.1 wt % and 0.3 wt % within quartz from the zebra type minerallisation and between 0.3 wt % and 0.7 wt % within vein type quartz, whereas within fluorite samples (Žune-Dolinac locality) it is between 0.4 and 0.5 wt %. Maximum SO_4^{2-} values up to 30,000 ppm (3 wt.%), were observed within a single fluorite sample. This very high concentration level, not confirmed by presence of gypsum or anhydrite in the fluid inclusions, (due to high Ca concentration), is most likely attributed to contamination (e.g., solid inclusions of barite) since barite is frequently found in the paragenesis. However, it also points to a significant change in the fluid chemistry responsible for the genesis of barite deposits, decreased depth of formation, and the increased contribution of sea water. A deficit of cations is observed in the vein-type quartz. This can be attributed to the presence of Fe^{2+} within the fluids, which was not measured during the procedure or to the absorption of divalent cations to the quartz powder during the crushing procedure.

The lithium content is highly elevated within zebra-type quartz and varies between 366 ppm and 2300 ppm, whereas for the vein type quartz it is in the range between 60 ppm and 150 ppm. Fluorite samples have uniform lithium concentrations varying between 325 ppm and 405 ppm. The presence of Li in the ore fluids was suspected by the extremely low eutectic temperature in quartz fluid inclusions from the zebra siderite down to -90 ºC.

High Li concentration in the leachates and the presence of dio-trioctachedral chlorites from the donbassite-tosudite-cookeite solid solution and $(LiAl_4(Si_3Al)O_{10}(OH)_8$ (Fig. 4C, SLOVENEC & PALINKAŠ, 2003) in the same cavity, confirms the high Li concentration in evaporitic bitter brines taking part in siderite genesis. This is one piece of evidence which connects evolved sea water from Permian evaporitic basins or lagoons with the ore forming process. High Li and B concentrations are common components in evaporitic bitter brines elsewhere (STEVEN & ZVI, 2011; 209 ppm, LIPPMANN et al.,1999). An additional contribution of Li may come from leaching of the surrounding host rocks, shales and sandstones. (McCAFFREY et al., 1987). CÉCILE et. al. (2002) consider high-salinity fluids, derived from sedimentary basins, responsible for the Li enrichment in FI-s in the barren quartz from the Spanish Central System (Sierra de Guadarrama). According to KRAUSKOPF (1982), the average shale contains 60 ppm of Li, twice that of the average granite.

Diagram Na/Cl vs. Cl/Br follows the sea water evaporation line. The measured ratios are the result of sea water evaporation rate between 12 and 36 % (Fig. 20A). It confirms the evaporation trend on all samples of zebra siderite, vein siderite, ankerite, quartz in siderite veins, vein barite and dark limestone. Galena exhibits very variable ratios. Galena associated with zebra siderite has Na^+ around the sea water composition, and in the vein siderite, above sea water on the evaporation line. It means a possible contribution of halite dissolution from evaporites. It should be mentioned that sulphide paragenesis in the cavities within zebra siderite is the last phase in the succession of dark siderite-light siderite-quartz-sphalerite-galena which suggests a prolonged time-span of ore formation.

The Ca_{excess} vs. $Na_{deficiency}$ diagram (Fig. 20B) shows a wide spectrum of contemporaneous ore forming processes which follow concurrently the metasomatism of Carboniferous limestones and dolostones by hydrotherms. The major trends are: (i) Ca_{excess} increases by metasomatism of carbonates, ankeritization and sideritization, and (ii) albitization of plagioclases (1 mole of Na for 1 mole of Ca).

The temperature of fluids was also calculated on the basis of geothermometric pairs: Na/K = 210-258 ºC (mean 184ºC); K/Mg = 261-443 ºC (mean 355ºC); Na/K/Ca = 280-441ºC (mean 328ºC); and Na/Li = 124-589ºC (mean 329ºC). The use of traditional geothermometric pairs which includes Ca and Mg, obtains unreliably high values. Their use is provided for water/fluid equilibria in the common aquifer rocks, while in the Ljubija geothermal field metasomatism excessively predominates other equilibrium processes. In contrast, the Na/K geothermometer gives reasonable temperature, although in geothermal and epithermal enviroments this geothermometer reflects the deep reservoir fluid/rock equilibration rather than the fluid inclusion entrapment temperature (SIMPSON et al., 2015).

5.5. VITRINITE REFLECTANCE

Nine of seventeen samples from the Tomašica locality are selected for vitrinite reflection: (i) 6 host limestones; (ii) phyllite (aleurolite, frequently used in the literature on Sana-Una. Palaeozoic lithology); (iii) siderite, and (iv) sulphide rich sediment, which all contained >0.5% of organic carbon. According to petrography, most of the samples are composed of amorphous organic matter (99-100%) with traces of vitrinite and rarely pyrobitumene. The exception is the sample composed of 70% amorphous organic matter and 30 % vitrinite. All samples show a high thermal alteration index (TAI ~ 4). The degree of vitrinite

Table 1. Ljubija/Adamuša

Sample	Mineralogy	Mineralisation type	Li^+ (meq/l)	Na^+ (meq/l)	K^+ (meq/l)	Mg^{2+} (meq/l)	Ca^{2+} (meg/l)	F^- (meg/l)	Cl^- (meg/l)	Br^- (meq/l)	I^- (meq/l)	NO_3^{2-} (meq/l)	SO_4^{2-} (meq/l)	Na (mol/l)
LJ 010/1	Quartz	Siderite, Zebra type	96	7481	609		1139	472	7584	22		119	145	325
Lj 011/1	Quartz	Siderite, Zebra type	22	10392	823		315	7	11119	42		162	75	452
Lj 014/1	Quartz	Siderite, Zebra type	103	10377	660		806	2	11425	43		74		451
PR-LJ-12	Quartz	Siderite, Vein type	11	5336	476	683	12465	34	9344	47	0.5	4318	1341	232
PR-LJ-13	Quartz	Siderite, Vein type	12	4391	452	581	12659	30	8381	27	0.6	998	454	191
PR-LJ-14	Quartz	Siderite, Vein type	16	3081	249	363	11748	9	5496	20	0.5	465	327	134
Lj 008/2	Siderite	Siderite, Zebra type	157	9834	544	2343	9419	32	14136	71		33	860	428
Lj 010/2	Siderite	Siderite, Zebra type	314	14459	863	3763	11172	27	23017	258		65	90	629
Lj 011/2	Siderite	Siderite, Zebra type	196	10099	761	4297	10995	33	15760	147		74	208	439
Lj 013/2	Siderite	Siderite, Zebra type	246	11236	732	3899	8741	27	18174	149		31		489
Lj/014/2	Siderite	Siderite, Zebra type	256	10226	570	4452	6635	7	16224	122		40		445
Lj 015/2	Siderite	Siderite, Zebra type	209	10527	505	4418	7271	19	16665	123		29		458
PR-LJ-1	Siderite	Siderite, Vein type	101	12534	544	6535	6337	145	30458	192	0.9	321	206	545
PR-LJ-4	Siderite	Siderite, Vein type	188	8812	1844	5275	16245	62	20489	231	0.6	196	3527	383
PR-LJ-5	Siderite	Siderite, Vein type	67	14884	856	741	1995	56	26356	114	1.7	820	<20	647
PR-LJ-9	Siderite	Siderite, Vein type	417	10468	458	7720	12683	43	25633	338	0.7	196	1129	455
Lj 009/2	Ankerite	Siderite, Zebra type	280	20159	735	10602	25392	20	31845	110		28	138	877
Lj S-4	Calcite	Hydrothermal calcite		216	46	268	16406	4	166			72	238	9
PR-LJ-3	Dark limestone	Host rock	62	3775	5269	2197	19779	227	6620	36	10.8	308	1358	164
PR-LJ-8	Dark limestone	Host rock	26	3032	436	1507	25951	121	4744	68	6.9	177	19065	132
PR-LJ-6	Barite	Siderite, Vein type	16	4943	319	616	14378		9658	50	0.8	118	3965	215
PR-LJ-7	Barite	Siderite, Vein type	3	3877	325	682	22685	46	8630	34	0.6	174	20654	169
Lj 012/3	Galena	Siderite, Zebra type	3	4659	293	178	1624	13	6673	8		114	1492	203
PR-LJ-2	Galena	Siderite, Vein type	4	5869	352	571	8487	126	10701	26	0.1	168	409	255
PR-LJ-11	Galena	Siderite, Vein type		1455	96	315	1711	31	2034		<0,1	163	2243	63
ŽUNE/DOLINAC														
Naziv	Mineral	Opis	Li^+ (meq/l)	Na^+ (meq/l)	K^+ (meq/l)	Mg^{2+} (meq/l)	Ca^{2+} (meg/l)	F^- (meg/l)	Cl^- (meg/l)	Br^- (meq/l)	I^- (meq/l)	NO_3^{2-} (meq/l)	$SO_4$2- (meq/l)	Na (mol/l)
DZ 1/I	Fluorite	Barite-fluorite vein	34	6316	1073	1256	9490	7351	11896	58		683	564	275
DZ 3/II	Fluorite	Barite-fluorite vein	40	8281	421	382	9626	7040	15072	52		308	701	360
DZ 3/III	Fluorite	Barite-fluorite vein	49	10793	825	306	9260	7703	19137	88		185	651	469
DZ 3/I	Fluorite	Barite-fluorite vein	53	8928	297	381	21709	6841	16199	50		156	494	388
DZ 3/II	Fluorite	Barite-fluorite vein	36	11963	436	277	8631	7895	13612	64		134	3343	520
DZ 100	Barite	Barite-fluorite vein		281	125	568	10824	982	257			269	10352	12
DZ 101	Barite	Barite-fluorite vein		373	167	169	3708	371	823			230	2815	16
DZ 102	Barite	Barite-fluorite vein		369	192		1839	130	779			197	2723	16
DZ 103	Barite	Barite-fluorite vein	15	9234	781	195	2374	52	18092	120		241	2133	402
PR-LJ-10	Barite	Barite-fluorite vein	395	47035	1353	14662	33533	60	76299	467	32.3	192	562	2046
PR-LJ-10A	Barite	Barite-fluorite vein		336	72	1358	21291	11	146		0.1	202	18953	15
LJ-10/A	Barite	Barite-fluorite vein	<1	57	24	<2000	12160	35	102		1.0	84	16698	2
DZ 106	Quartz	Barite-fluorite vein	10	5065	537	262	5088	8	5804	27		609	823	220
DZ 107	Quartz	Barite-fluorite vein		3272	448		2248	8	3367	15		545	1109	142

reflection within the limestones is represented by Ro of 4.0 – 4.6%. Using the diagram T-R_o-t (time of effective heating, maximum temperature, vitrinite reflectance) gives a temperature of 200-210 ºC (BOSTICK et al., 1979) and 247-258 ºC after (BERKER & PAWLEWITZ, 1994); The sample of limestone with pyrobitumen has an Ro of 4.6%, which appropriates to a temperature of 210 ºC and 258 ºC, respectively. Within phyllites with 30% vitrinite, R_o of 4.8 %, gives T of 215 ºC and 262 ºC, by two methods. Sediments with sulphides, where R_o = 3.7%, appropriate to T of 193 ºC and 228 ºC. A siderite sample with R_o 3.2% gives T of 193ºC and 228ºC.

The temperatues obtained are in good agreement with the fluid inclusion data, $T_{boiling}$ 240ºC, and Na/K, where T is 210-258 ºC.

5.6. SULPHUR ISOTOPES

Sulphur isotope compositions were determined on sulphides and sulfates. Sulfur isotopic data are presented in Table 2 (STRMIĆ PALINKAŠ, 2004). The $\delta^{34}S$ values of the sulphides increases in order to 3.0 ‰) ≤ chalcopyrite ≤ (-0.8 to +2.3 ‰) ≤sphalerite (+0.4 to +4.4 ‰) < pyrite (+5.4 to +8.5 ‰). There was no distinction perceived between sulphides separated from dark siderite and zebra ore. The $\delta^{34}S$ values of barite samples (+9.2 to ± 0.2 ‰ V-CDT) fall within the range of the latest Permian marine evaporites (HOLSER & KAPLAN, 1966). The temperature of cogenetic geothermometric pairs was calculated by the constants given by OHMOTO & RYE (1979). The calculated temperature suggests the absence of isotopic equilibria. The reasonable temperature of 245ºC was

Table 1. Ljubija/Adamuša

Cl (mol/l)	**Br (mol/l)**	**Ca (mol/l)**	**Na/Br (mol)**	**evapor. (%)**	**Cl/Br (mol)**	**evapor. (%)**	**GEOT. Na/K (oC)**	**GEOT. K2/Mg (oC)**	**GEOT. Na/K/ Ca b=1/3 (oC)**	**GEOT. Na/Li Cl<0.3M (oC)**	**GEOT. Na/Li Cl>0.3M (oC)**	**Ca/Na**	**Mg/Na**	**Caex (meq/l)**	**Nadef (meq/l)**
214	0.28	28.42	1162	0.0	764	0.0	188.9		373.4	177.0	373.2	0.2		49.7	-142.1
314	0.53	7.87	857	0.0	595	12.0	186.7		407.7	64.6	190.0	0.0		5.2	-183.3
322	0.54	20.11	838	0.0	598	12.0	171.6		364.6	156.1	337.8	0.1		29.4	-175.2
264	0.59	311.03	393	15.0	446	15.1	195.8	392.0	330.2	64.0	189.1	2.3	0.1	613.2	-6.2
236	0.34	315.86	558	9.0	690	0.0	207.6	394.6	337.4	77.1	209.6	2.9	0.1	623.8	11.6
155	0.24	293.12	549	9.0	635	0.0	188.3	364.3	305.2	113.5	267.5	3.8	0.1	581.0	-1.2
399	0.89	235.03	481	10.7	449	15.5	163.0	352.6	309.2	195.6	405.2	1.0	0.2	456.7	-86.0
649	3.23	278.76	195	23.6	201	35.0	167.6	370.3	325.3	225.7	458.0	0.8	0.3	535.7	-72.5
445	1.83	274.34	239	20.4	242	26.8	183.2	355.0	336.5	214.4	438.1	1.1	0.4	533.8	-58.3
513	1.87	218.09	262	20.0	275	24.0	173.2	355.8	329.5	226.3	459.0	0.8	0.3	419.0	-49.4
458	1.53	165.56	290	19.0	299	23.0	163.4	332.1	316.3	240.6	484.7	0.6	0.4	315.8	-52.6
470	1.54	181.41	296	19.0	304	23.1	154.8	323.7	302.3	216.7	442.0	0.7	0.4	347.1	-55.0
859	2.40	158.12	227	21.0	358	20.1	149.6	315.4	300.8	141.2	313.0	0.5	0.5	287.4	191.1
578	2.89	405.34	133	30.0	200	35.0	281.4	422.3	441.0	223.6	454.3	1.8	0.6	791.3	112.0
743	1.43	49.78	454	12.0	521	12.0	165.3	443.4	350.9	103.2	251.0	0.1		74.6	-10.3
723	4.23	316.46	108	36.0	171	40.4	150.0	298.3	286.4	297.1	589.0	1.2	0.7	608.7	164.3
898	1.38	633.57	636	0.0	651	10.5	141.2	319.4	280.0	183.6	384.5	1.3	0.5	1237.0	-107.1
5		409.35					284.3	261.6	308.1			76.0	1.2	818.5	-5.4
187	0.45	493.51	367	15.0	417	16.4				198.6	410.4	5.2	0.6	980.7	-4.2
134	0.85	647.52	155	27.0	157	44.8	239.0	352.4	346.6	145.1	319.5	8.6	0.5	1290.5	-17.2
272	0.63	358.76	341	16.0	432	16.3	172.6	363.1	296.5	85.6	223.0	2.9	0.1	708.4	18.5
243	0.43	566.03	393	14.9	567	12.0	191.0	360.4	305.4	27.6	133.2	5.9	0.2	1123.9	40.0
188	0.10	40.52	2009	0.0	1866	0.0	170.9	408.8	325.0	20.9	123.0	0.3	0.0	74.7	-41.3
302	0.33	211.76	775	0.0	916	0.0	167.9	374.2	302.7	21.5	124.0	1.4	0.1	413.4	3.4
57		42.70					174.3	301.1	294.2			1.2	0.2	83.5	-14.1
						MEAN:	**184.7**	**355.3**	**328.1**	**148.7**	**329.5**	**4.8**	**0.4**		
ŽUNE/DOLINAC															
Cl (mol/l)	Br (mol/l)	Ca (mol/l)	Na/Br (mol)	evapor. (%)	Cl/Br (mol)	evapor. (%)	GEOT. Na/K (oC)	GEOT. K2/Mg (oC)	GEOT. Na/K/ Ca b=1/3 (oC)	GEOT. Na/Li Cl<0.3M (oC)	GEOT. Na/Li Cl>0.3M (oC)	Ca/Na	Mg/Na	Caex (meq/l)	Nadef (meq/l)
336	0.73	236.80	379	14.0	463	15.1	257.0	439.6	411.4	113.5	267.7	1.5	0.2	462.3	12.8
425	0.65	240.18	551	9.0	650	10.5	158.1	407.1	296.5	107.3	257.5	1.2		466.1	4.2
540	1.10	231.06	428	13.2	492	13.2	184.2	486.8	343.0	103.5	251.4	0.9		444.0	-6.8
457	0.63	541.67	617	0.0	726	0.0	137.2	376.8	254.1	120.0	278.2	2.4		1068.0	3.2
384	0.80	215.37	651	0.0	480	13.2	141.2	425.4	280.5	80.5	214.9	0.7		417.9	-191.3
7		270.08					390.1	298.8	399.8			38.6	2.0	539.9	-6.0
23		92.52					391.0	362.9	434.7			10.0	0.5	184.3	3.7
22		45.89										5.0		91.0	2.8
510	1.50	59.22	268	19.0	340	20.4	191.7	506.6	371.8	52.5	171.2	0.3		101.3	35.7
2152	5.85	836.68	350	15.0	368	20.5	131.2	352.1	279.9	143.7	317.2	0.7	0.3	1601.2	-201.5
4		531.24					284.3	241.6	317.5			63.3	4.0	1062.3	-11.1
3		303.42					379.8		333.7			212.4		606.7	-0.0
164	0.33	126.94	661	0.0	491	13.2	210.3	448.9	361.0	60.4	183.5	1.0	0.1	248.4	-80.0
95	0.19	56.10	757	0.0	505	13.0	234.2		388.3			0.7		109.0	-60.9
						MEAN:	**237.7**	**395.1**	**344.0**	**97.7**	**242.7**	**24.2**	**1.2**		

obtained by galena-sphalerite pair from cavities in the zebra siderite calculated by the equation of KIYOSU (1973) and FRIEDMAN & O'NEIL (1977). The $\Delta^{34}S_{sulphide\text{-}sulphate}$ vs. $\delta^{34}S_{sulphide}$ diagram enabled determination of the $\delta^{34}S_{\Sigma S,}$ $R = X_{SO4}/X_{H2S}$ by the equation after OHMOTO (1986). A determined value of +9.2 ‰ V-CDT supports the evolution of Permian sea water by evaporation as the main sulphur source. Sulphur isotope values of sulphates were not affected by thermochemical reduction, it explains a low fugacity of sulfur and small quantity of sulfides including pyrite in the overall area. Some contribution from the decomposition of organically-bound sulphur and oxidation of pyrite from the sedimenary host rocks, dark coloured clastics, are not excluded (Fig. 21).

5.7. GEOCHRONOLOGY

K/Ar dating

K/Ar dating was performed on the following samples: (i) 5 phyllites from the Trnava locality; (ii) 6 phyllites from the Blagaj locality; (iii) 6 phyllites from the Adamuša locality, 4 of them are fragments associated within vein-type siderite mineralization; (iv) a single phyllite sample from the Tomašica locality; (v) single phyllite sample from Jezero locality; (vi) limestone undissolved residuum from the Adamuša locality, and (vii) 9 samples of rhyolite rocks from the Trnava locality.

Whole rock phyllite samples (4 samples) from the Trnava locality contain between 1.3 and 3.6 % of potassium and gave an age between 171.3±6.6 and 195.4±7.5 Ma, whereas a single

mica concentrate (4.2 % of potassium) gave an age of 212.0±8.0 Ma. Whole rock phyllite samples (4 samples) from the Blagaj locality (1.2 to 3.6 % of potassium) gave an age between 214.2±8.3 and 233.1±9.4 Ma, whereas two mica concentrates (4.2 % of potassium) gave an age of 188.7±7.1 and 193.7±7.3 Ma. Two whole rock phyllite samples (1.2 and 4.0 % of potassium) gave ages of 290.0±11.0 Ma and 283.4±10.6 Ma, respectively. Additional 4 whole rock phyllites associated with vein-type siderite mineralization (0.7 to 3.6 % of K) yielded ages between 200.0±9.0 and 236.0±9.0 Ma. A whole rock phyllite sample from the Tomašica locality contains 1.5 % of K and gave an age of 238.7±9.2 Ma, whereas a whole rock phyllite sample from the Jezero locality (3.9 % of K) yielded an age of 132.9±5.1 Ma. Whole rock analysis of the undissolved residuum of the limestone of the Adamuša locality (2.1 % of K) gave an age of 220±10.0 Ma.

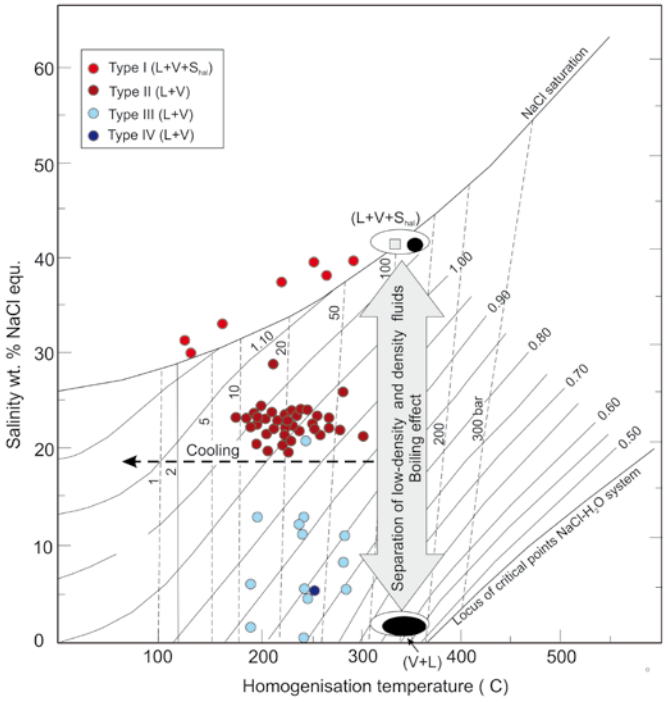

Figure 19. Temperature of homogenization (Th) vs. salinity diagram for the inclusions in the fluorite from the Žune-Dolinac barite-fluorite vein deposit. The span of Th and salinities reflects the evolution of P-T-X condition during boiling.

Table 2. Sulphur isotope data of sulphides and sulphates from the Ljubija ore deposits.

Sample	Mineralogy	$\delta^{34}S$ (‰ V-CDT)
JS-LJ-100-1	Galena	-0.5
JS-LJ-101-1	Pyrite	7.6
JS-LJ-104-1	Sphalerite	0.8
JS-LJ-104-2	Chalcopyrite	2.3
JS-LJ-104-3	Chalcopyrite	1.2
JS-LJ-105-1	Pyrite	6.5
JS-LJ-106-1	Pyrite	8.5
JS-LJ-106-4	Pyrite	6.7
JS-LJ-107-1	Galena	-1.3
JS-LJ-107-2	Barite	9.3
JS-LJ-108-1	Galena	-0.4
JS-LJ- 109-1	Sphalerite	4.4
JS-LJ-109-2	Barite	9.2
JS-LJ-109-3	Galena	3
JS-LJ-112-1	Sphalerite	0.8
JS-LJ-113-1	Sphalerite	0.4
JS-LJ-113-4	Galena	-2.3
JS-LJ-113-5	Chalcopyrite	-0.8

Whole rock rhyolite samples (9 samples) of the Trnava locality contain from 0.1 to 2.0 % potassium with an age range from 56.6±4.3 to 237.0±9.5 Ma.

Wide spectrum of data from 56 Ma to 290 Ma on phyllites and volcanics shows different degrees of loss of radiogenic Ar, due to long-term tectonism and associated thermal events in the polyphase metamorphic evolution of the Dinarides (PALINKAŠ & PECSKAY, 1996, unpublished, Fig. 22).

The first group (i), (283-290 Ma), belongs to the post-Variscan thermal event in Lower Permian time, connected with an incipient intra-continental rifting stage. It corresponds to the post-Variscan ages determined in the Mid-Bosnian Schists Mts. (PAMIĆ et al., 2004). The group (ii) varies widely (175-238 Ma) and represents disturbed ages by the later tectono-thermal events, as indicated by the $^{40}Ar/^{39}Ar$ dating. The third group (iii) with a Lower Cretaceous overprint (98-132 Ma) is most likely a result of later resetting in a tectonically active zone. It has a regional significance and marks obduction related tectonism and metamorphism, traditionally named the Eoalpine, which started 130 Ma ago (HSÜ, 1989). This Lower Cretaceous overprint is recognized on the Silurian-Devonian metamorphic complex on the Medvednica Mts. (110-122 Ma), (BELAK et al., 1996), on the Drina-Ivanjica Palaeozoic block in Serbia (129-139), (MILOVANOVIĆ, 1984), and in the metarhyolites in the Mid-Bosnian Schist Mts. (92-121), (PAMIĆ et al., 2004). The group (iv), younger Palaeocene overprint (56-64 Ma) determined on volcanics, corresponds to the Palaeocene early collision stage between Africa (Adria) and Euroasia (Tisia-Moesia), the cause of the Dinaride uplift in the Eocene. PAMIĆ & PÉCSKAY (1996) reported Late Cretaceous K/Ar ages of 94.3 and 85.4 Ma from basalt and diabase from the northwestern side of the Medvednica Mts.

$^{40}Ar/^{39}Ar$ analysis

$^{40}Ar/^{39}Ar$ analysis is performed on the low potassium white mica concentrate (paragonitic white mica), from phyllite fragments associated with the vein type of mineralization. The white mica concentrate yields a strongly disturbed pattern. The low-energy steps of the age spectrum show significant excess argon and an age of 340 Ma, whereas high energy steps gave a plateau-type of age at 275 Ma constituting together 96.7 percent of ^{39}Ar (steps 2-4, Fig. 23; BOROJEVIĆ ŠOŠTARIĆ, 2009). $^{40}Ar/^{39}Ar$ released spectra could be interpreted in another way. The plateau age of 340 Ma might be an inherited Variscan age (Lower Carboniferous) of the sedi-

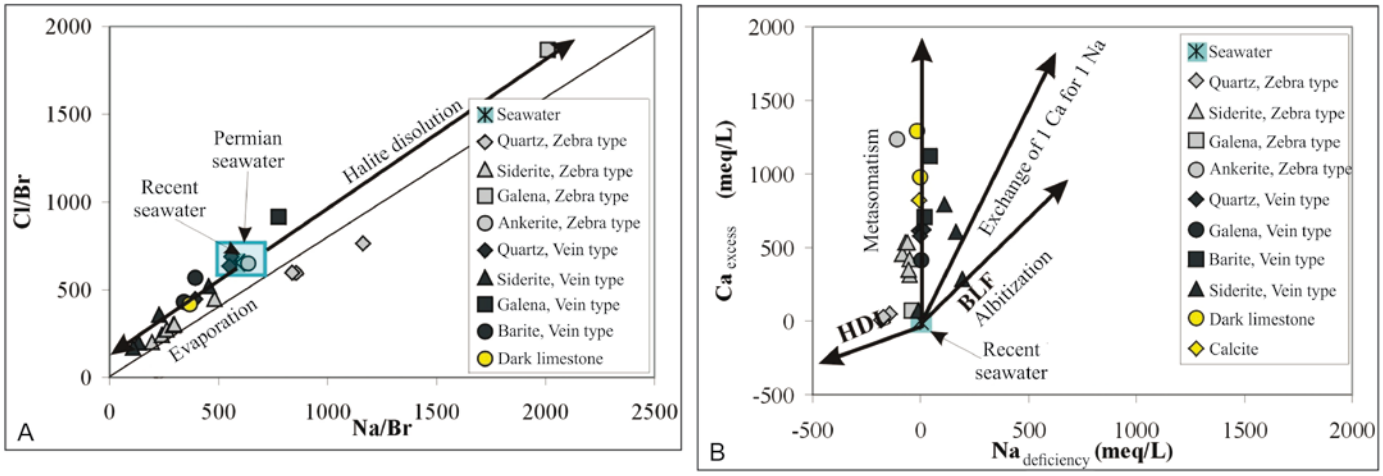

Figure 20. A) Diagram showing Na/Cl/Br variation of fluids extracted as leachates from the ore and host minerals. Most of data follow the evaporation trend, and only a few the trend of halite dissolution, the Ljubija/Adamuša ore deposit; B) Diagram Ca access vs. Na deficiency with theoretical trends of fluid evolution. Legend: HDL halite dissolution line; BLF line of basinal fluids; zebra siderite, banded texture; vein mesothermal siderite; dark limestones, footwall of the ore mineralization.

ment, precursor of phyllite, overprinted by a Lower Permian thermal event.

A white mica concentrate from the phyllite, sample LJUB 1, from the Palaeozoic Sana-Una Unit yielded a plateau age of 335.1 ± 23.1 Ma comprising 96.8 percent of ^{39}Ar released. The inverse isochrone plots show a slightly disturbed initial ^{40}Ar/^{36}Ar ratio of 322± 27 Ma, and an age of 327±30 Ma, together constituting 100 percent of ^{39}Ar released (BOROJEVIĆ ŠOŠTARIĆ, 2012).

6. ORE GENESIS

Genesis of the Ljubija ore deposits was a subject of controversy. The basic interpretation models have two approaches (i) a syn-sedimentary stratiform type with an obscure origin of iron, and the alternative (II) hydrothermal replacement and epigenetic vein type. To solve the dilemma, in the past decades a number of analytical procedures and methodologies have been applied in building a convincing genetic model. There was a number of ambiguities which obscured the solution, and paved the ground for unsupported genetic hypotheses. The objective approach requires resolution of the following particularities: textural-structural characteristics, time of formation, source of metal, pressure, temperature and chemistry of the ore forming fluids, alterations, and not least, the metallogenic affiliation to the equivalent deposits in the frame of plate tectonic divisions and reconstruction of the Dinarides, and the wider area within the Neotethyan domain.

6.1. TEXTURAL-STRUCTURAL CHARACTERISTICS

The Fe mineralisation in the Ljubija ore field comprises stratabound siderite and ankerite bodies hosted by Carboniferous limestones, and siderite-sulphide veins placed within organic rich shales. PALINKAŠ (1988) recognized three major types of primary iron ore textures: (1) dark massive siderite and ankerite, and (2) zebra siderite composed of dark massive and light sparry siderite bands, and (3) sparry siderite veins hosted clastics (Figs. 3, 4, 5).

Ore microscopy and transmitted light microscopy offer a visual observation of metasomatic processes (Figs. 8, 9). The textural type (1) was formed by the metasomatic replacement of dark massive limestone by dark massive siderite. The differences between massive siderite (1) and zebra siderite texture (2) were the result of chemical kinetics controlled by temperature, acidity buffered by the host rocks, and salinity. All these parameters have been reasserted by the research data (PALINKAŠ et al., 2003b; STRMIĆ PALINKAŠ, 2004, 2009; BOROJEVIĆ ŠOŠTARIĆ, 2004).

When the dissolution volumetric rate of calcite was equal to the precipitation volumetric rate of siderite, the primary texture was retained, i.e. dark metasomatical Fe-carbonate was precipitated. In contrast, when the volumetric rate of dissolution was higher than the rate of precipitation, cavities are formed and the primary texture is lost. Further supply of mineralizing fluid caused crystallization of light sparry siderite directly from solution (STRMIĆ PALINKAŠ, 2004).

The genesis of three textural types has been ascertained by the chemistry of metasomatic processes, (STRMIĆ PALINKAŠ, 2004; STRMIĆ PALINKAŠ et al., 2009) through the following contributions: (i) Variations in δ^{13}C values of the barren and mineralized carbonates suggest the progressive replacement, and depositional character of vein siderite; (ii) The δ^{18}O values of siderite and the calcite vein from dark massive siderite give a value of isotope equilibrium temperature, $T_{isotope}$ = 224 ºC; (iii) The δ^{18}O values of siderite and quartz pairs from siderite veins give $T_{isotope}$ = 168 ºC; (iv) The δ^{34}S values of sphalerite and galena pairs from zebra ore give $T_{isotope}$ = 245 ºC; (v) The δ^{34}S value of barite falls within the range of contemporaneous Permian sea water; (vi) Barren massive limestones have a negative Ce_N anomaly and negative Eu_N typical of marine carbonates;(vi) Positive Eu_N in siderite indicates precipitation in a low-temperature environment (<250 ºC) from fluid which received their REE signature during fluid/rock interactions in a high temperature environment. A combination of positive Eu_N and negative Ce_N anomalies is inconceivable in sedimentary siderite; (vii) Vein siderite has a negative Eu_N due to its precipitation from fluids depleted from Eu; (viii) The pristine/phitane ratio higher than 1

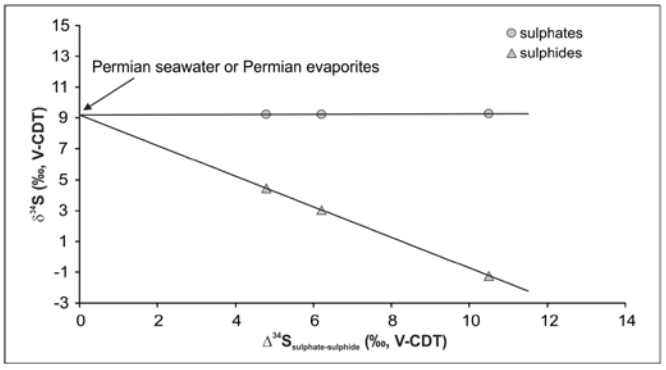

Figure 21. $\Delta^{34}S_{sulphide\text{-}sulphate}$ vs. $\delta^{34}S_{sulphide}$ digram for coexisting sulphates and sulphides. The measured value at +9.2 ‰ V-CDT suggests an evaporative-evolved Permian sea water as the main sulphur source.

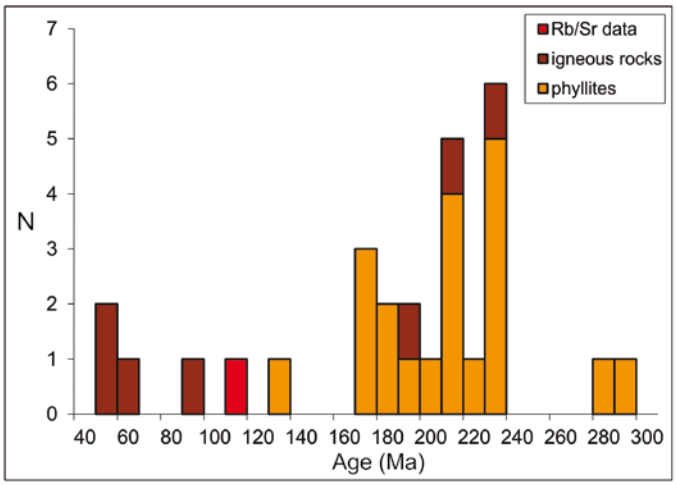

Figure 22. The range of $^{40}Ar/^{39}K$ values determined on 21 samples of phyllites and 7 samples of volcanics from the Sana-Una Palaeozoic area (PALINKAŠ & PECSKAY, 1996, unpub.).

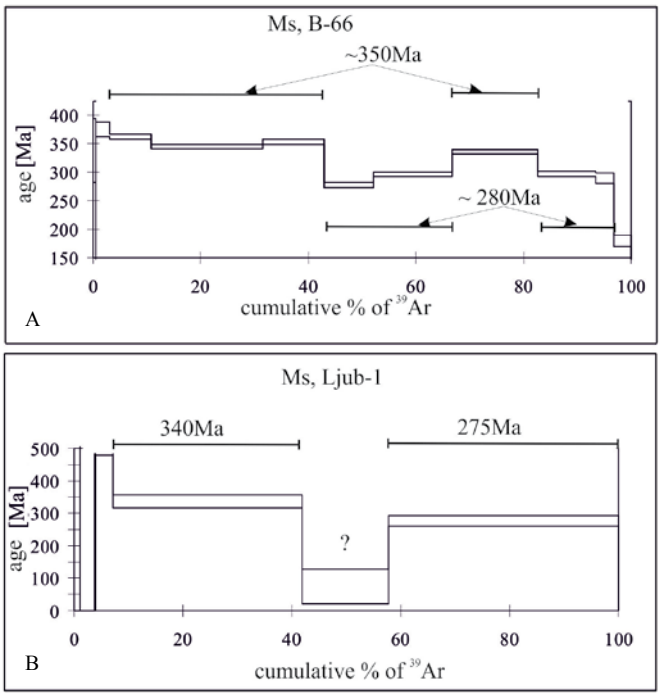

Figure 23. The $^{40}Ar/^{39}Ar$ analyses, performed on the low potassium white mica concentrate from phyllite fragments associated with the vein type of mineralization, yielded two ages, the low energy step of 340 Ma, and a high energy step with a plateau age of 275 Ma (Fig. 23B). The first, Variscan age of 340 Ma, is overprinted by an Early Permian tectono-thermal event dated at 275 Ma. These pairs of ages bear regional significance and are repeated steadily in the neighbouring area of the Sana-Una Palaeozoic, in the Trgovska gora and Petrova gora ore districts hosted by the Carboniferous sediments. $^{40}Ar/^{39}Ar$ released spectra show Variscan plateau ages at 332.8±3.1 Ma and 342.9±3.3 Ma, overprinted by a thermal event at ca. 265.6±6.2 to 274.2±3.1 Ma, interpreted as a maximum age of the hydrothermal activity (Fig. 23A, BOROJEVIĆ-ŠOŠTARIĆ et al., 2009).

in the barren and mineralized samples points to an oxic depositional environment for the host rock carbonates, an inconvenient condition for the synsedimentary deposition of siderite ore. A reducing environment during diagenesis, controlled by indigenous organic matter, however, is a prerequisite for epigenetic metasomatic sideritization.

6.2. TEMPERATURE AND CHEMISTRY OF FLUIDS

Study of fluid inclusions in quartz from three textural siderite types and within the siderite itself from the ore deposit Adamuša/Ljubija, and fluorite from the fluorite-barite deposit Žune-Dolinac supported by crush-leach analysis and vitrinate reflectance, paved the way to substantial information on ore forming fluids, their temperature and composition.

The ore forming fluids with highly variable salinities (2-39 wt% NaCl equiv., Adamuša/Ljubija; 5-33.4 wt% NaCl equiv., Žune-Dolinac), are essentially modified sea water derived through different degrees of evaporation in lagoons, up to the point of halite precipitation (the evaporation line on the diagram Na/Cl vs Cl/Br). Boiling phenomena, observed and determined on fluid inclusions, contributed to the variable salinity of fluids, which underwent distillation (boiling evaporation), at the topmost position of the cell, near the land surface. The boiling temperature was controlled by hydrostatic pressure at depths of 100-200 m below the land surface.

The hydrothermal solution in fluid inclusions is primarily represented by NaCl-H_2O and NaCl-$CaCl_2$±$MgCl_2$-H_2O systems. Ca^{2+} and Mg^{2+} ions are evidence of the widespread metasomatic replacement of limestones and dolomites by Fe^{2+} (Ca_{excess} vs. $Na_{deficiency}$ diagram).

The high concentration of Li^+ ions in leachates, and the presence of cookeite, $(LiAl_4(Si_3Al)_{10}(OH)_8)$ as an alteration mineral, confirm the engagement of chloride rich evaporitic sea water, responsible for the mobilization of metasomatic Fe^{2+} from shale, but some proportion comes from leaching of Li-rich mica. The SO_4^{2-} ion, recorded in leachates, was essential for deposition of the ubiquitous barite deposits. In spite of a slight variation, the $\delta^{34}S$ values of barite around +9.2‰ V-CDT, the $\delta^{34}S_{barite}$ value bears witness to Permian sea water as a dominant water supplier in the circulation cell. The minor thermochemical reduction of sulphate was the source of HS^- for sulphide deposition.

Thermal characteristics of the ore forming fluids are confirmed by the study of fluid inclusions (Th, 100-275ºC), Na/K ratio in leachates (141-281ºC), vitrinite reflectance (210-260ºC) and stable isotope geothermometers (164-224ºC). This overall range of temperatures could be more specific in a sketch presen-

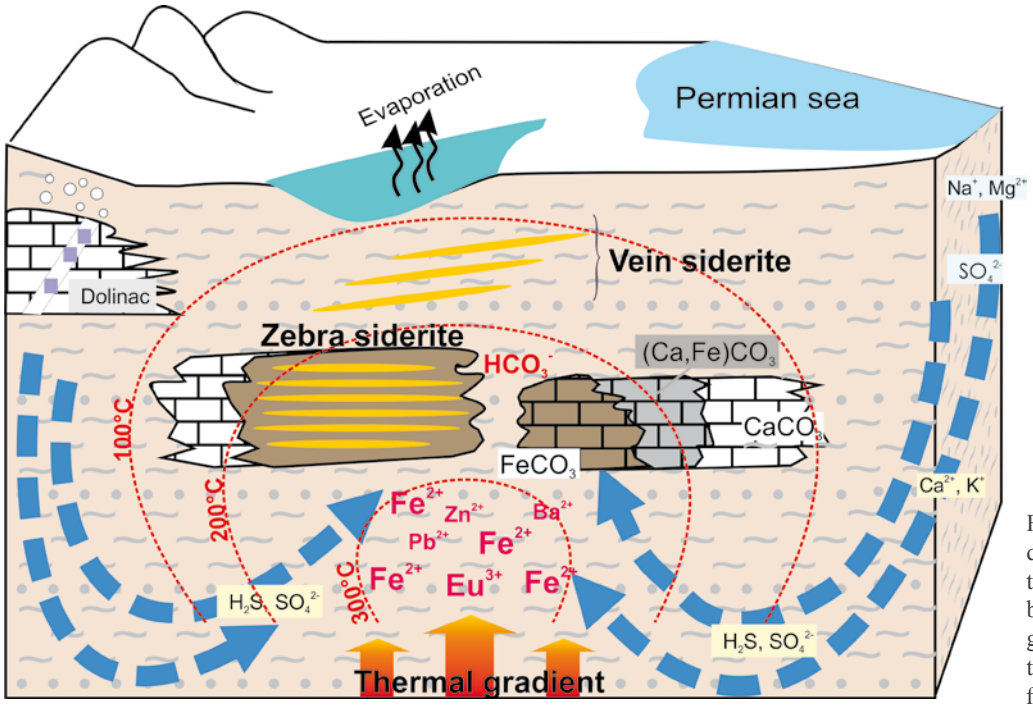

Figure 24. Metasomatic-hydrothermal genetic model of the Ljubija mineral deposits based on inorganic and organic geochemical data. Shape of isotherms depict local heat foci and fluid flow in a geothermal field.

tation of thermal distribution in the hydrothermal circulation cell (Fig. 24).

The shape of the circulation cells, formed over the foci of high heat flow, at the Adamuša/Ljubija deposit, is defined by the position of isotherms reconstructed by the temperature of mineral formation. The chemical zonation is accompanied by thermal zonation. The highest trapping temperature and salinities are registered at the lower position of the cell, in the quartz of the zebra metasomatic siderite (salinity 35-39 wt% NaCl equiv., Th 215-275ºC). The lowest temperature and salinity are measured in the quartz in siderite veins in the uppermost part of the cell (salinity 2-9 wt% NaCl equiv., Th 100-250ºC). The plume of heat controls the shape and the character of fluids from high salinity bitter brines at deeper parts of the cell, to the diluted aliquots, with lower salinity, supplied by normal sea or meteoric water. The wide range of temperatures suggest mixing of hot-high salinity water FLUID 1 and cold-low salinity waters FLUID 2 (Fig. 13, diagram T_h vs. salinity).

The Žune-Dolinac barite-fluorite deposit (like the other numerous barite deposits in the Ljubija geothermal field) experienced intensive boiling due to their near-surface setting.

6.3. TIME OF MINERALIZATION

Age determination relied on indirect methods, available during research, (i) $^{39}K/^{40}Ar$, (ii) $^{40}Ar/^{39}Ar$, and (iii) origin of sulphur in the ore mineralization implied through its isotope signature.

The K/Ar blocking temperatures, determined on phyllites, indicate four significant thermal events. The group (i), (283-290 Ma), belongs to the post-Variscan thermal event in Lower Permian time, connected with the incipient intra-continental rifting stage. The group varies widely (175-238 Ma) and represents disturbed ages by the later tectono-thermal events. The third group (iii) with a Lower Cretaceous overprint (98-132 Ma) is most likely a result of later resetting in a tectonically active zone. The group (iv), younger Palaeocene overprint (56-64 Ma) determined on the volcanics, corresponds to a Palaeocene early collisional stage between Africa (Adria) and Eurasia (Tisia-Moesia). The first group (i) on the Carboniferous phyllites is of primordial significance in the polyphase metamorphic history of the Tethys (Fig. 22). (ii) The $^{40}Ar/^{39}Ar$ analyses, performed on the low potassium white mica concentrate from phyllite fragments associated with the vein type of mineralization, yielded two ages, the low energy step of 340 Ma, and a high energy step with a plateau age of 275 Ma. The first, Variscan age of 340 Ma, is overprinted by an Early Permian tectono-thermal event dated at 275 Ma. These pairs of ages bear regional significance and are repeated steadily in the neighbouring area of the Sana-Una Palaeozoic, in the Trgovska gora and Petrova gora ore districts hosted by the Carboniferous sediments. ^{40}Ar-^{39}Ar released spectra show Variscan plateau ages at 332.8±3.1 Ma and 342.9±3.3 Ma, overprinted by a thermal event at ca. 265.6±6.2 to 274.2±3.1 Ma, interpreted as a maximum age of the hydrothermal activity (Fig. 23). The Middle Permian age of mineralisation is corroborated by the following arguments: (i) The mineralisation is hosted exclusively within Carboniferous to Early Permian units. (ii) Sulphur isotopes show a Permian seawater signature, while the increased bromine content of the leachates points to evaporated seawater not to the evaporites themselves, as a source of sulphates. (iii) The $^{40}Ar/^{39}Ar$ spectra recorded thermal overprints at 265.6±6.2 and 274.2±3.1 Ma for Petrova gora and at 298.0±4.2 Ma for Trgovska gora, superimposed exclusively onto the Variscan ages of the host rock.

6.4. LJUBIJA GEOTHERMAL FIELD

The Ljubija ore deposits were formed within the Ljubija geothermal field which extends into the Trgovska gora and Petrova gora Palaeozoic terrains. The Ljubija geothermal field deserves the term "*geothermal field*" by because of the areal extension of its ore deposits of several hundred square kilometres over the Sana-Una Palaeozoic. The Ljubija geothermal field incorporates a huge accumulation of Fe-carbonate, sulphide, barite and fluorite

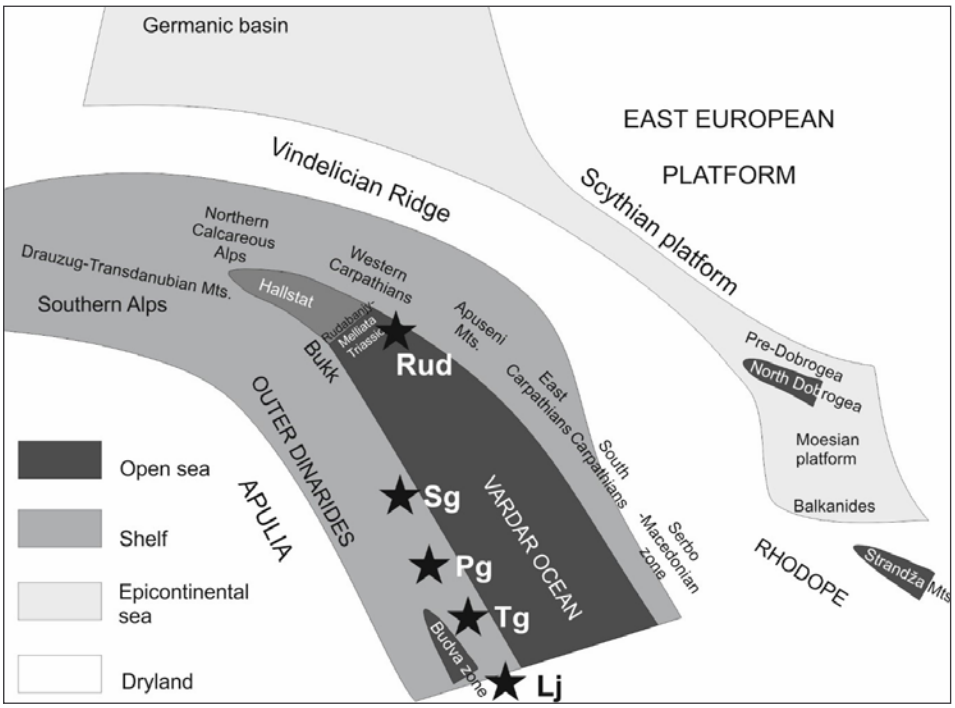

Figure 25. Palinspastic sketch shows the North Hungarian Triassic units, with special regard to Ladinian palaeogeography (not to scale), KOVÁCS (1984). The sketch depicts advanced rifting in progress toward the Northwest (present geographical orientation), dissecting Pangea into the Gondwanian and Eurasian continental blocks. Early rifting formations and phenomena, including Permo-Carboniferous geothermal fields, were covered by newly formed Dinaridic and Moesian carbonate platforms,. Tectonic evolution, uplift, napping, thrusting and erosion uncovered their mineral load to the present exposed situation. Abbreviations: R.-M. Lj Ljubija, Tg Trgovska gora, Pg Petrova gora, Sg Samoborska gora, Rud Rudabánya.

mineralisation, with almost half a billion tonnes of Fe ore, at the Adamuša/Ljubija, Tomašica, and Omarska ore districts. The chemistry, pressure and temperature of the thermal waters enriched in Ca, Mg, Na, chloride and bromine, are common in rifting-related fluids elsewhere (e.g., HARDI, 1990; ROWLAND & SIBSON, 2004; SIMPSON et al., 2015). The general characteristics of the Ljubija geothermal field corresponds in many aspects to the Salton sea geothermal field, an active rifting environment, regarding composition and temperature of Ca rich brines, metaliferous sediments, etc. (CRAIG, 1966; SKINNER et al., 1967).

Due to the initial phase of rifting, the crust in the passive margin was thinner than adjacent crust, and geothermal systems developed at high heat flow foci along an elongated rifting zone and fractures controlled convection circulation systems. Here the geothermal water had been circulating to considerable depth (> 1 km), through mostly vertical fractures, to extract the heat from the rocks.

SAEMUNDSSON (2009) classified geothermal systems on the basis of geological setting, reservoir temperature and enthalpy: (i) Low-temperature systems with reservoir temperatures at 1 km depth below 150°C; (ii) Medium-temperature systems with reservoir temperature at 1 km depth between 150- 200°C; (iii) High-temperature systems with reservoir temperature at 1 km depth above 200°C, with reservoir fluid enthalpies greater than 800 $kJkg^{-1}$.

The pressure-temperature characteristics of the Ljubija geothermal field are closer to the (iii) High temperature system. The Ljubija geothermal field was water dominated, and at places, to varying degrees, vapour dominated. The enthalpy content in the two-phase boiling system in Žune-Dolinac was close to 982 $kJkg^{-1}$ for the liquid phase and 2877 $kJkg^{-1}$ for the developing vapour phase (data for the temperature of 245°C and salinity of 33 wt. % NaCl).

Carboniferous and Permian formations were cap rocks (total thickness of 600-800 m), a blanketing seal of the geothermal system and their rock formation were the object of metasomatic sideritization. The rifting fault zones provided conduits for fluid flow and heat flow, and hydraulic pressure forces fluids to the surface forming hot springs, fumaroles, etc., in the boiling zone, at places were the temperature and pressure followed the boiling point curve and where steam and water coexisted.

The barite-fluorite vein deposit of Žune/Dolinac is a feeder zone of one of the many hot springs. Thermal gradients calculated on the basis of hot hydrothermal water, issuing on the surface, and colder Permo-carboniferous host rocks are not a convenient place to calculate a regional geothermal gradient. A proper geothermal gradiant, providing the thermal water, is in the aquifer reservoir below the Carboniferous and Permian formations.

As initial rifting proceeded, listric fault systems formed and further subsidence resulted in the creation of a Red sea type basin, developed by the formation of the Neo-Tethyan ocean crust. Equivalent types of huge siderite-barite-polysulfide mineralisations are situated within the similar geotectonic environment, however, with a much more complex tectono-thermal history in the course of the Alpine orogeny. The siderite mineralisation with similar characteristics, in low to medium grade metamorphic Variscan basement units, has been studied in the Western Carpathians and Eastern Alps (GRECULA et al.,1995; HURAI et al., 2002, 2008a; RADVANEC et al., 2004; URBAN et al., 2006; HURAI et al., 2008b, b; POHL, 1986; LAUBE et al., 1995; PROCHASKA & HAFELLNER, 1994), EBNER et al. (1999). The origin and age of this mineralisation is still under discussion. As a corollary, the Ljubija geothermal field is a herald for the birth of the Tethyan Ocean and the onset of the new Alpine Wilson cycle.

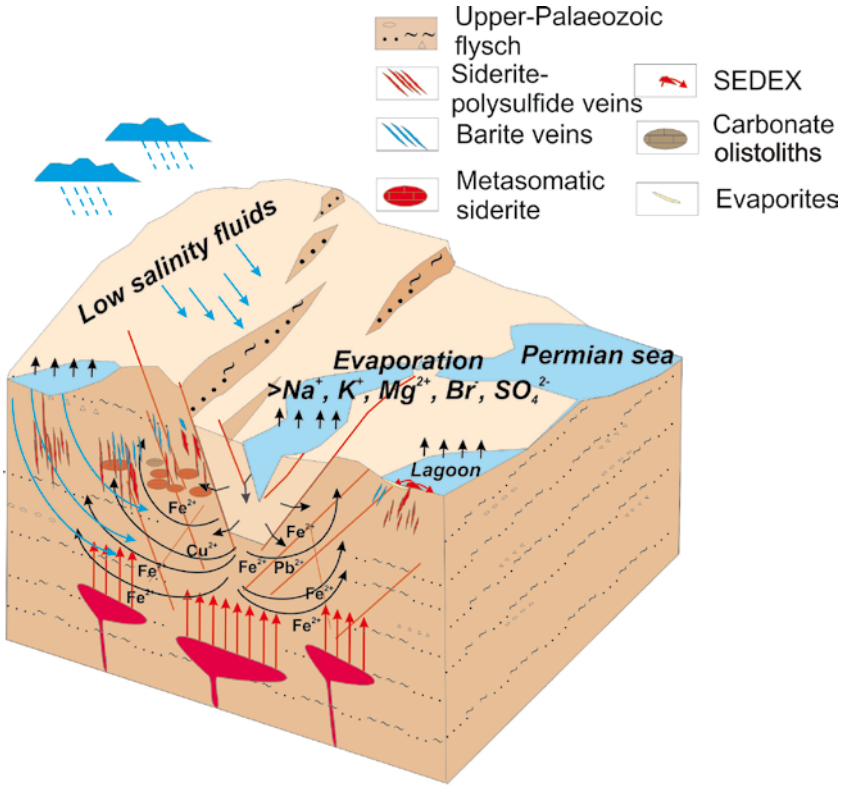

Figure 26. A simplified genetic model of the Permian siderite-barite-polysulphide deposits, Ljubija, Trgovska gora, Petrova gora, Samoborska gora, Bistra-Medvednica, presently placed along the Dinaridic carbonate platform, within the Palaeozoic of the Inner Dinarides. As initial rifting proceeded and listric fault systems formed, further subsidence resulted in the creation of a Red sea type basin, developing into the Tethyan oceanic crust in Late Triassic time. The high heat flow in the early rifting structures created an array of circulating hydrothermal cells.

Reconstruction of the opening scenario which loosely defines space, time and related geotectonic events is depicted on the palinspastic sketch of the North Hungarian Triassic units, with special reference to Ladinian palaeogeography (not to scale!), (Fig. 25, KOVÁCS, 1984). The sketch portrays advanced rifting in progress toward the northwest (present geographical orientation) dissecting Pangea into the Gondwana and Eurasian continental blocks. Early rifting formations and Permo-Carboniferous geothermal fields, were covered by newly growing Dinaridic and Moesian carbonate platforms on the opposite sides of divergent, drifting continental margins (PALINKAŠ et al., 2016, this publication). Tectonic evolution, uplift, napping, thrusting and erosion uncovered their mineral load to the present exposed situation.

7. SUMMARY

The Ljubija ore deposits are situated within the thick Upper Palaeozoic sequence of the allochthonous Sana-Una Palaeozoic complex of the Inner Dinarides. The primary ore occurs as stratabound metasomatic bodies of iron carbonates within Carboniferous limestones and dolostones, and siderite veins within the Carboniferous phyllites and metasandstones.

Primary mineralization consists of siderite-ankerite-barite-polysulphides with three textural types, dark massive siderite, zebra siderite, alternation of dark and light siderite bends with sulphide cavities, and open space fillings in the veins. The shape of the cell is defined by isotherms based on mineral formation temperature, tentatively. The most influential processes in the formation of chemical components of fluids are metasomatic sideritization and ankeritization. The ore forming fluids are dominantly NaCl-$CaCl_2$-H_2O, with highly variable salinity (0.4 to 39 wt% NaCl equiv.) and T_h between 100 and 310ºC. The hydrothermal fluids are a mixture of high-temperature-high-salinity Permian evaporitic sea water, diluted by low-temperature-low-salinity sea or meteoric waters. Boiling of near-surface hydrothermal reservoirs contributed to the high variability of temperature and salinity of the fluids. Sulphur isotopes confirm Permian sea water as the major source of sulphates ($\delta^{34}S$ +9.2 ‰ V-CDT) for barite formation. Thermal reduction of marine sulphates supplies HS^- for the precipitation of sulphides, which were deposited out of equilibria, with the exception of the cogenetic pair galena-sphalerite, formed at 245ºC. The temperature of formation determined by oxygen isotopes on calcite-siderite-quartz cogenetic mineral pairs is in the range between 164º to 224ºC. Temperatures of the cation geothermometer (Na/K) matches those obtained from fluid inclusion, vitrinite reflectance and isotope thermometry.

The age determination recorded two prominent tectonothermal events, Variscan (332.8±3.1 Ma and 342.9±3.3 Ma), overprinted by a thermal post-Variscan event at ca. 265.6±6.2 to 274.2±3.1 Ma, and interpreted as the maximum age of hydrothermal activity in the Middle Permian.

The ages and thermal features coincide well with those in the neighbouring deposits in the Palaeozoic of Trgovska gora and the Petrova gora Mts., its counterparts in space and time, announcing the future break-up of Pangea and the birth of Tethys (Fig. 26).

Acknowledgement

This study was mostly supported by the Croatian Ministry of Sciences, Technology and Sports (Projects 119-0982709-1175). We are grateful to Tamara TROSKOT and Darko ŠPANIĆ (INA oil company) for valuable vitrinite reflection analyses, Prof. Ronald J. BAKKER (Montanuniversität, Leoben, Austria) for

providing access to the Raman spectrometry facilities, to Štefica KAMPIĆ for assistance in the lab work, to Nenad RAKOVIĆ and Zorana SLJEPČEVIĆ (ArcelorMittal, Ljubija mining company) for the field assistance during numerous visits with or without students. We would like to thank reviewers, Ferenc MOLNAR and Todor SERAFIMOVSKI, whose comments greatly improved the presentation and clarity of the paper.

REFERENCES

BAKKER, R.J. (2003): Package FLUIDS 1. Computer programs for analysis of fluid inclusion data and for modelling bulk fluid properties.– Chem Geol, 194, 3–23. doi: 10.1016/S0009-2541(02)00268-1

BAKKER, R.J. (1991): Adaption of Bowers & Helgeson (1983) equation of state to isochore and fugacity coeficient calculation in the H_2O-CO_2-CH_4-N_2-NaCl fluid system.– Chem Geol, 154, 225–236.

BELAK, M., JAMIČIĆ, D., CRNKO, J. & SREMAC, J. (1995): Niskometamorfne stijene zelenih ortoškriljavaca i paraškriljavaca na cesti Runolist-Željezničar (Low-metamorphic rocks, greenschists, ortometamorphic and parametamorphic on the road Runolist-Željezničar.– In: ŠIKIĆ, K. (ed.): Geološki vodič Medvednice (Geological guide on Medvednica), Geol Inst, Zagreb, 104–107, Zagreb.

BERKER, C.E. & PAWLEVICZ, M.J. (1994): Calculation of Vitrinite Reflectance from Thermal Histories and Peak Temperature. A Comparison of Methods.– In: MUKHOPADHAY, P.K. & DOW, W.G. (eds): Vitrinite reflectance as a maturity parameter: application and limitations. Am Chem Soc ACS, Symp ser, 570, 216–229. Washington.

BOROJEVIĆ ŠOŠTARIĆ, S. (2004): Geneza sideritno-baritno-polisulfidnih rudnih ležišta u paleozoiku Unutrašnjih Dinarida (Genesis of siderite-barite-polysulfide ore deposits in Palaeozoic of the Inner Dinarides).– Master thesis, University of Zagreb, p. 120.

BOROJEVIĆ ŠOŠTARIĆ, S., PALINKAŠ, A.L., STRMIĆ PALINKAŠ, S., BERMANEC, V., NEUBAUER, F., SPANGENBERG, J.E. & PROCHASKA, W. (2009): Origin of siderite–barite-polysulfide mineralisation in Petrova and Trgovska Gora Mts., NW Dinarides.– Miner Petrol, 97, 111–128.

BOROJEVIĆ ŠOŠTARIĆ, S., NEUBAUER, F., HANDLER, R & PALINKAŠ, L.A. (2012). Tectonothermal history of the basement rocks within the NW Dinarides: new 40Ar/39Ar ages and synthesis.– Geol Carpath, 63, 6, 441–452.

BOSTICK, N.H., CASHMAN, S.M., McCULLOH, T.H. & WADDEL, C.T. (1979): Gradients of vitrinite reflectance and present temperature in the Los Angeles and Ventura Basin, California.– In: OLITZ, DF. (ed.): Low temperature metamorphism of kerogen and clay minerals. Soc Econ Paleont Miner, Pacific Sec, 65–96, Los Angeles.

BOTTRELL, S.H., YARDLEY, B.W.D. & BUCLEY, F. (1988): A modified crush-leach method for the analysis of fluid inclusion electrolytes.– Bull Mineral, 11, 279–290.

BURKHARD, M. (1993): Calcite twins, their geometry, apearance and significance as stress-strain markers and indicators of tectonic regime: a review.– J Struc Geol, 15, 351–368.

CAN, I. (2002): A new improved Na/K geothermometer by artificial neutral networks.– Geothermics, 31, 751–760.

CHANNEL, J.E.T., D'ARGENIO, B. & HORVATH, F. (1979): Adria, the African promontory in Mesozoic Mediterranean paleogeography.– Earth-Sci Rev., 15, 213–202.

CISSARZ, A. (1951): Die Stellung der Lagerstätten Jugoslaviens im geologischen Raum.– Geološki vesnik IX, 23–60.

COLLINS, PLF. (1979): Gas hydrates in CO2 bearing fluid inclusions and the use of freezing data to estimating of salinity.– Econ Geol, 74, 1435–1444.

CRAIG, H. (1966): Isotopic Composition and Origin of the Red Sea and Salton Sea Geothermal Brines.– Science, 154, 3756, 1544–1548. doi: 10.1126/science.154.3756.1544

CVIJIĆ, R. (2001): Mineralni resursi željeza, pelitoidne rude Ljubijske metalogenetske oblasti i perspektive razvoja (Iron ore resources, pelitoid ore of the Ljubija metallogenic province and development), (in Serbian with English summary).– Fac Min Geol, Belgrade, p. 154.

CVIJIĆ, R. (2004): Geomenađment u funkciji korišćenja i razvoja mineralnih resursa Ljubijske metalogenetske oblasti (Geomanagement in the function of utility and development of mineral resources in the Ljubija metallogenic district).– Rudarski Institut, Prijedor, p. 348.

DAVIES, D.W., LOWENSTEIN, T.K. & SPENCER, R.J. (1990): Melting behavior of fluid inclusions in laboratory-grown halite crystals in the systems NaCl-H_2O, NaCl-KCl-H_2O, NaCl-$MgCl_2$-H_2O, and NaCl-$CaCl_2$-H_2O.– Geochim Cosmochim Ac, 54, 591–601. doi: 10.1016/0016-7037(90)90355-O

DAVISSON, M.L. & CRISS, R.E. (1996): Na-Ca-Cl relations in basinal fluids.– Geochim Cosmoshim Ac, 60/15, 2743–2752. doi: 10.1016/0016-7037(96)00143-3

DERCOURT, J., RICOU, L.E., & VRIELYNCK, B. (1993): Atlas Tethys Paleoenviromental Maps.– Gauthiers-Villars, Paris. 307 p.

ĐEREKOVIĆ, B., MAKSIMČEV, S., KUJUNDŽIĆ, S., SUNARIĆ, O., HOHRAJN, J., KOVAČEVIĆ, R., KAČAR, B., VELJKOVIĆ, R., JOJIĆ, D., MARIĆ, LJ., LOŽAJIĆ, M., PAMIĆ, J., KAPELER, I., ĐORĐEVIĆ, D. & JURIĆ, M. (1976): OGK SFRJ 1:100 000, map Prijedor, Feder Geol Survey, Belgrade.

CÉCILE, F., BOIRON, M.C., DUBESSY, J., CHABIRON, A., CHAROY, B., & CRESPOT M. (2002): Advances in lithium analysis in solids by means of laser-induced breakdown spectroscopy: an exploratory study.– Geochim Cosmochim Ac, 66, 8, 1401–1407.

EBNER, F., CERNY, I., EICHORN, R., GÖTZINGER, M., PAAR, W., PROCHASKA, W., & WEBER, L. (2000): Mineral Resources in the Eastern Alps and Adjoining area.– In: NEUBAUER & HÖCK (eds): Aspects of Geology in Austria, Miner Österr Geol Ges, 92, 157–184.

FERRIL, D.A., MORRIS, P.A., EVANS, M.A., BURKHARD, M., GROSHONG, Jr R.H., ONASH, C.M, (2004): Calcite twin morphology: a low-temperature deformation geothermometer.– J Str Geol, 26, 1521–1529. doi: 10.1016/j.jsg.2003.11.028

FOURNIER, R.O. & TRUESDELL, A.H. (1973): An empirical Na-K-Ca geothermometer for natural waters.– Geochim Cosmochim Ac, 37, 1255–1275. doi: 10.1016/0016-7037(73)90060-4

FRIDMAN, I. & O'NEIL, JR. (1977): Compilation of stable isotope fractionation factors of geochemical interest.– US Geol Sur Am Bull, 63, 325–380.

GIGGENBACH, W.F. (1988): Geothermal solute equilibria. Derivation of Na-K-Mg-Ca geoindicators.– Geochim Cosmochim Ac, 52, 2749–2765. doi: 10.1016/0016-7037(88)90143-3

GRECULA, P., ABONYI, A., ABONYIOVÁ, M., ANTAŠ, J., BARTALSKÝ, B., BARTALSKÝ, J., DIANIŠKA, I, DRNZÍK, E., ĬUĬA, R., GARGULÁK, M., GAZDAČKO, L., KOBULSKÝ, J., LÖRINCZ, L., MACKO, J., NÁVESÒÁK, D., NÉMETH, Z., NOVOTNÝ, L., RADVANEC, M., ROJKOVIČ, I., ROZLOŽNÍK, L., ROZLOŽNÍK, O., VARČEK, C. & ZLOCHA, J. (1995): Mineral deposits of the Slovak Ore Mountains.– Miner Slovaca, Monograph, 1, Bratislava, 834 p.

GRUBIĆ A., PROTIĆ L.J., FILIPOVIĆ, I. & JOVANOVIĆ, D. (2000): New data on the Palaeozoic of the Sana-Una Area.– Proceedings of the International Symposium of the Dinarides and the Vardar Zone. Acad Sci Art Rep Serb, Dept Natur Math and Tech Sci I, Banja Luka, 49–54.

GRUBIĆ, A. & CVIJIĆ, R. (2003): New contribution in Geology and Metallogeny of the Ljubija Iron Ore Mine.– Mining Inst., Prijedor, 137 p.

GRUBIĆ, A. & PROTIĆ L.J. (2003): Novi prilozi za geologiju i metalogeniju rudnika gvozdja Ljubija. GRUBIĆ, A. & CVIJIĆ, P. (eds.): Mining Inst, Prijedor, 1–137.

HAAS, J.L. (1971): The effect of salinity on the maximum thermal gradient of hydothermal system at hydrostatic pressure.– Econ Geol, 66, 940–946.

HAAS, J.L. (1976): Thermodynamic Properties of the Coexisting Phases and Thermochemical Properties of the NaCl Component in Boiling NaCl Solutions.– Geol Survey Bull, 1421-B.

HARDI, L.A. (1990): The roles of rifting and hydrothermal CaCl2 brines in the origin of potash evaporites: an hypothesis.– Am J Sci, 290, 43–106.

HEINRICH, C. & NEUBAUER, F. (2002): Cu–Au–Pb–Zn–Ag metallogeny of the Alpine- Balkan-Carpathian-Dinaride geodynamic province.– Min Deposita 37, 533–540.

HOLSER, W.T. & KAPLAN, I.R. (1966): Isotope geochemistry of sedimentary sulfates.– Chem Geol, 1, 93–135. doi: 10.1016/0009-2541(66)90011-8

HORITA, J., FRIEDMAN, T.J., LAZAR, B. & HOLLAND, H.D. (1991): The composition of Permian seawater.– Geochim Cosmochim Ac, 55, 417–432. doi: 10.1016/0016-7037(91)90001-L

HORVATH, F. & D'ARGENIO, B. (1985): Subsidance history and tectonics of western Adria margin.– Ac Geol Hun, 28/(1–2), 109–117.

HOSIENI K., REED A.H. & SCANLON M.W. (1985): Thermodynamics of the lambda transition and the equation of state of quartz.– Am Mineral, 70,782–793.

HSÜ, KJ. (1989): Time and place in Alpine orogenesis-the Fermor lectures.– Geo Soc S P, 45, 421–443. doi: 10.1144/GSL.SP.1989.045.01.23

HURAI, V., HARČOVA, E., HURAIOVA, M., OZDIN, D., PROCHASKA, W. & WIEGEROVA, V. (2002): Origin of siderite veins in the Western Carpathians I. P-T-Xδ^{13}C-δ^{18}O relations in ore forming brines of the Rudnany deposits.– Ore Geol Rev, 21, 67–101.

HURAI, V., LEXA O., SCHULMANN, K., MONTIGNY, R., PROCHASKA, W., FRANK, W, KONECNY., P, KRÁL J., THOMAS, R. & CHOVAN, M. (2008a): Mobilization of ore fluids during Alpine metamorphism: evidence from hydrothermal veins in the Variscan basement of Western Carpathians, Slovakia.– Geofluids, 8, 181–207. doi: 10.1111/j.1468-8123.2008.00216.x

HURAI, V., PROCHASKA, W., LEXA, O., SCHULMANN, K., THOMAS, R. & IVAN, P. (2008b): High-density nitrogen inclusions in barite from a giant siderite vein: implications for Alpine evolution of the Variscan basement of Western Carpathians, Slovakia.– J Metamorph Geol, 26, 487–498. doi: 10.1111/j.1525-1314.2008.00775.x

JANKOVIĆ, S. (1977): Major Alpine metallogenic units in the northeastern Mediterranean and concepts of plate tectonics.– In: JANKOVIĆ, S. (ed.):

Metallogeny and Plate Tectonics in the Northeastern Mediterranean. IGCP-UNESCO, Correlation program, vol. 3, Fac Mining Geol, Belgrade, 105–172.

JANKOVIĆ, S. (1987): Genetic types of the Alpine ore deposits and their tectonic settings in the Northeastern Mediterranean and Southwest Asia.– In: PETRASCHEK, W.E. & JANKOVIĆ, S. (eds.): Geotectonic Evolution and Metallogeny of the Mediterranean Area and Western Asia. IGCP 169, Springer-Verlag, Wien, 23–36. doi: 10.1007/978-3-7091-5822-7_2

JEREMIĆ, M. (1958): Baritno-fluoritno ležište Žune kod Ljubije (Barite-fluorite deposit Žune-Dolinac near Ljubija, in Serbian).– Rudarsko-metalurški zbornik, 4, Ljubljana.

JEREMIĆ, M. (1959): Baritonosno područje Une i Sane u sjeverozapadnoj Bosni (Barite bearing region within the Una and Sana rivers in northwest Bosnia, in Serbian).– Rudarstvo i metalurgija, 2, Belgrad.

JURKOVIĆ, I. (2003): Metallogeny of Southern Tisia–Moslavačka gora Mt., and Mts. Psunj, Papuk, Krndija.– Rudarsko-geološko-naftni zbornik, 15, 1–17 (in Croatian).

JURKOVIĆ, I. (1961): Minerali željeznih rudnih ležišta Ljubije kod Prijedora (Mineralogical investigation of iron ore deposits Ljubija near Prijedor in Bosnia, in Croation with English summary).– Geološki vjesnik, 14, 161–220.

JURIĆ, M. (1971): Geologija područja sanskog paleozoika u sjeverozapadnoj Bosni (Geology of Sana Palaeozoic, NW Bosnia; in Croation).– Geološki glasnik, XI, Sarajevo, p. 146.

KIYOSU, Y. (1973): Sulfur isotope fractionation among sphalerite, galena and sulfide ions.– Geochem J, 7, 191–199.

KARAMATA S., KRSTIĆ B., DIMITRIJEVIĆ M.D., DIMITRIJEVIĆ M.N., KNEŽEVIĆ V., STOJANOV, R. & FILIPOVIĆ, I. (1997): Terranes between the Moesian Plate and the Adriatic Sea.– Ann Geol Pays Hellén, 37, (1996/97), 429–477.

KATZER, F. (1910): Die Eisenerz lagerstätten Bosniens und der Herzegovina, Manzsche Hof: Universitäts - Buchhandlung, Vienna, 343 p.

KATZER, F. (1925): Geologie Bosniens und der Herzegovina. Direkcija državnih rudarskih poduzeća. Sarajevo, p. 520.

KORZHINSKII, D.S. (1968): The theory of metasomatic zoning.– Miner Deposita, 3, 222–231. doi: 10.1007/BF00207435

KOVACS, S. (1984): North Hungarian Triassic facies types: a review.– Ac Geol Hun, 27, (34), 251–264.

KRSTIĆ, B., FILIPOVIĆ I., MASLAREVIĆ L.J., SUDAR, M. & ERCEGOVAC, M. (2005): Carboniferous of the Central Part of Balkan Peninsula.– Bull T CXXX, Acad Serbe Sci Art, Cl. Sci Math Nat, Sci Nat, 43, 41–56.

LAUBE, N., FRIMMEL, H.E. & HOERNES, S. (1995): Oxygen and carbon isotopic study on the genesis of the Steirischer Erzberg siderite deposit (Austria).– Miner Deposita, 30, 285– 293. doi: 10.1007/BF00196364

LIPPMANN, M., TRUESDELL, A. & FRYE, G. (1999): The Cerros Prieto and Salton Sea geothermal fields- are they really alike?– Proceedings of the 24th Workshop on Geothermal Reservoir Engineering, Stanford University, Stanford, California, 25–27.

LUDWIG, K.R. (2001): Using Isoplot/Ex, Version 2.01: A geochronological, toolkit for Microsoft Excel.– Berkeley Geochronology Center, Spec P 1a, Berkeley, 47 p.

LUDWIG, K.R. (2005): Isoplot/EX rev. 3.32: A geochronological toolkit for Microsoft Excel.– Berkeley Geochronology Center Spec P 4, Berkeley.

McCAFFERY, M.A., LAZAR, B. & HOLLAND, H.D. (1987): The evaporation path of seawater and the coprecipitation of Br^- and K^+ with halite.– J Sediment Petrol, 57, 928–937.

MERINO, E., CANALS, A. & FLETCHER. R.C. (2006): Genesis of self-organized zebra textures in burial dolomites: Diplacives veins, induced stresses, and dolomititzation.– Geol Acta, vol. 4, 3, 383–393.

MILOVANOVIĆ, D. (1984): Petrologija stena niskog stepena metamorfizma iz središnjeg dela Drina-Ivanjica paleozoika (Petrology of low-metamorphic rocks from the Middle part of Drina-Ivanjica Palaeozoic; in Serbian).– Glas Pri muz srp zemlje, (Bull. Museum Serb Lands), 39, 1–139, Belgrade.

NADEN, J. (1996): Calcic Brine: a Microsoft Excel 5.0 Add-in for calculating salinities from microthermometric data in the system NaCl−CaCl2−H2O.– In: BROWN P.E, HAGEMANN, S.G (eds): PACROFI VI, Pan Am Conf Res Fluid Inclusion: Madison Proceed, 97–98.

NÖTH (1952): Die Eisenerzlagerstätten Jugoslawiens. Belgrade.

OHMOTO, H. & RYE, R.O. (1979): Isotopes of Sulfur and Carbon.– In: BARNES H.L (ed.): Geochemistry of Hydrothermal Ore Deposits. Wiley-Intersci Pub, 509–561, New York.

OHMOTO, H. & LASAGA, A. (1982): Kinetics of reactions between aqueous sulfates and sulfides in hydtothermal systems.– Geochim Cosmochim Ac, 46/10, 1727–1745.

OLIVER, N.H.S. & BONS, P.D. (2001): Mechanisms of fluid flow and fluid rock interaction in fossil metamorphic hydrothermal systems inferred from vein-wallrock patterns, geometry and microstructure.– Geofluids, 1, 137–162. doi: 10.1046/j.1468-8123.2001.00013.x

PETRASCHECK, W.E. (1977): Some basic problems of metallogeny and plate tectonics in the Eastern Mediterranean.– In: JANKOVIĆ, S. (ed): Metallogeny and Plate Tectonics in the Northeastern Mediterranean. IGCP-UNESCO, Corr program, Vol 3, Fac Min Geol, Belgrade, 193–200.

PALINKAŠ, A.L. (1985): Lead isotopes patterns in galenas from some selected ore deposits in Croatia and NW Bosnia.– Geološki vjesnik, 38, 175–189.

PALINKAŠ, A.L. (1988): Geokemijske karakteristike paleozojskih metalogenetskih područja: Samoborska gora, Gorski Kotar, Lika, Kordun i Banija (Geochemical characteristics of Palaeozoic metallogenic regions: Samoborska gora, Gorski Kotar, Lika, Kordun and Banija, in Croatian with English summary).– Diss, Uni Zagreb, 108 p.

PALINKAŠ, A.L. (1990): Siderite-barite-polysulfide deposits and early continental rifting in Dinarides.– Geološki vjesnik, 43, 181–185.

PALINKAŠ, A.L., BOROJEVIĆ, S., PROCHASKA, W., ŠINKOVEC, B. & ŠIFTAR, D. (2000): Rude Samobor, siderite-hematite-polysulfide-barite mineral deposit within the Zagorje-Mid-Transdanubian Zone, NW Croatia.– In: TOMLJENOVIĆ, B., BALEN, D. & SAFTIĆ, B. (eds): Vijesti, Abstracts, Proc. PANCARDI 2000, Dubrovnik, 37/3, 96–98.

PALINKAŠ, A.L., BOROJEVIĆ, S., PROCHASKA, W., ŠINKOVEC, B. & ŠIFTAR, D. (2001): Rude Samobor deposit as a prototype of siderite-barite-polysulfide-hematite mineralization in the Inner Dinarides, Croatia.– In: PIESTRZYNSKI, A. (ed): Mineral Deposits at the Beginning of the 21st Century. Proc. Joint 6th Biennial SGA-SEG Meeting, Krakow, Poland, Balkema Rotterdam, 317–320.

PALINKAŠ, A.L., BOROJEVIĆ, S., STRMIĆ, S., PROCHASKA, W. & SPANGENBERG, J.E. (2003a): Siderite-hematite-barite-polysulfide mineral deposits related to the Early intracontinental Tethyan rifting, Inner Dinarides.– In: ELIOPOULOS et al. (eds): Mineral Exploration and Sustainable Development, Millpress, Rotterdam, 1225–1228.

PALINKAŠ, A.L., BOROJEVIĆ ŠOŠTARIĆ, S., STRMIĆ PALINKAŠ, S., BALOGH, K., PROCHASKA, W. & ŠIFTAR, D. (2003b): Ljubija siderite ore field, NW Bosnia, a precursor of the Early intra-continental rifting of the Tethys.– In: NEUBAUER & HANDLER (eds.): Geodynamics and Ore Deposit Evolution of the Alpine-Balkan-Carpathian-Dinaride province. Proc. of the Final GEODE-ABCD workshop. Seggauberg, Austria, Uni Salzburg, p. 65.

PALINKAŠ, A.L., BOROJEVIĆ ŠOŠTARIĆ, S., STRMIĆ PALINKAŠ, S., PROCHASKA, W. & CUNA, S. (2010): Permian polysulfide-siderite-barite-haematite deposit Rude in Samoborska Gora Mts., Zagorje-Mid-Transdanubian zone of Internal Dinarides.– Geol Croat, 63/1, 93–115. doi: 10.4154/GC.2010.06

PALINKAŠ, A.L., STRMIĆ, S., GARAŠIĆ, V., JURKOVIĆ, I. & MAJER, V. (2001): Permian metarhyolites and related ore deposits, Central Bosnia. Abstracts of the GEODE Workshop.– Romanian Jour Mineral Deposits, 79, 75–76.

PALINKAŠ, A.L., BOROJEVIĆ ŠOŠTARIĆ, S., STRMIĆ PALINKAŠ, S., CRNJAKOVIĆ, M., NEUBAUER, F., MOLNAR, F. & BERMANEC, V. (2010): Volcanoes in the Adriatic Sea: Permo-Triassic magmatism on the Adriatic-Dinaric carbonate platform.– Acta Mineralogica-Petrographica, 8, 1–15.

PAMIĆ, J. (1984): Triassic Magmatism of the Dinarides in Yugoslavia.– Tectonophysics, 109, 273–307. doi: 10.1016/0040-1951(84)90145-8

PAMIĆ, J. & PÉCSKAY, Z. 1996: Geological and K/Ar ages of Tertiary volcanic formations from the southern part of the Panonian Basin in Croatia – based on surface and subsurface data.– Nafta, 47, 195–202, Zagreb.

PAMIĆ, J. & JURKOVIĆ, I. (1997): Alpine magmatic-metallogenic formations of the Northwestern and Central dinarides.– Rudarsko-Geološko-Naftni zbornik, 9, 1–9.

PAMIĆ, J., GUŠIĆ, J. & JELASKA, V. (1998): Geodynamic evolution of the Central Dinarides.– Tectonophysics, 297, 251–268.

PAMIĆ, J., BALOGH, K., HRVATOVIĆ, H., BALEN, D., JURKOVIĆ, I. & PALINKAŠ, A.L. (2004): Ar and Ar-Ar dating of the Palaeozoic metamorphic complex from the Mid-Bosnian Schist Mts., Central Dinarides in Bosnia and Herzegovina.– Miner Petrol, 82, 65–89.

PAVLOVIĆ, P. (2004): Evaluation of the potential of Salar del Rincon brine deposit as a source of lithium, potash, boron and other mineral resources.– Unpublished report, for Argentina Diamonds Ltd.

POHL, W. (1986) Comparative metallogeny of siderite deposits.– Öst Schrift Erdwiss Komm, Wien, 8, 271–282. doi: 10.1007/978-3-7091-5822-7_22

PROCHASKA, W. & HAFELLNER, M. (1994) Pretertiary Siderite Mineralization In The Eastern Alps.– In: GRECULA, P. & NEMETH, Z. (eds.): Variscan Metallogeny in the Alpine Orogenic Belt. Proc. Inter Conf, Stará Lesná, Slovakia, p. 17.

PROCHASKA, W. (1997): Formation of different siderite provinces during the Alpine tectono-metamorphic events in the Eastern Alps of Austria.– In: PAPUNEN (ed.): Mineral deposits: research and exploration – where do they meet? Proc. 4th Biennial SGA Meeting, Turku, Finland, Balkema Rotterdam, 845–848.

RADVANEC, M., GRECULA, P. & ŽÁK, K. (2004): Siderite mineralization of the Gemericum superunit (Western Carpathians, Slovakia): review and a revised genetic model.– Ore Geol Rev, 24, 267–298. doi: 10.1016/j.oregeorev.2003.07.004

RAMOVIĆ (1957): Pregled olovno-cinčanih ležišta Bosne i Hercegovine (The review of lead and zinc mineral deposits in Bosnia and Herzegovina; in Bosnian).– Geološki glasnik, Sarajevo, 3, 5–124.

ROEDDER, E. (1984): Fluid inclusions.– Reviews in Mineralogy. Miner Soc Am, 12, 644 p., Washington.

ROTTURA, A., BARGOSSI, G.M, CAGGIANELLI, A., DEL MORO, A., VISONA, D., & TRANNE, C.A. (1998): Origin and significance of the Permian high-K calc-alkaline magmatism in the central-eastern Southern Alps, Italy.– Lithos, 45, 329–348. doi: 10.1016/S0024-4937(98)00038-3

ROWLAND, J.V. & SIBSON, R.H. (2001): Extensional fault kinematics within the Taupo Volcanic Zone, New Zealand: soft-linked segmentation of a continental rift system.– N Zeal J Geol Geop, 44, 271–283. doi: 10.1080/00288306.2001.9514938

SAERL, A. (1989): Saddle dolomite: a new view of its nature and origin.– Miner Mag, 53, 547–555. doi: 10.1180/minmag.1989.053.373.05

SAEMUNDSSON (2009): Exploration for Geothermal Resources, geothermal systems in global perspective geothermal training programme organized by UNU-GTP, Kenya.

SHEPERD, T.J., RANKIN, AH. & ALDERTON, D.H.M. (1985): A practical guide to fluid inclusion studies.– Blackie & Son Ltd., Glasgow, 239 p.

SIBLEY, D.F. & GREGG, J.M. (1987): Classification of dolomite rock.– J Sediment Petrol, 57, 6967–975.

SIMPSON, M.P., STRMIC PALINKAS, S., MAUK, J.L. & BODNAR, R.J. (2015): Fluid inclusion chemistry of adularia-sericite epithermal Au-Ag deposits of the southern Hauraki Goldfield, New Zealand.– Econ Geol, 110, 763–786. doi: 10.2113/econgeo.110.3.763

SKINNER, B.J., ROSE, H.J. & MAYS, R.E. (1967): Sulfides associated with the Salton Sea geothermal brine.– Econ Geol, 62/3, 316–330. doi: 10.2113/gsecongeo.62.3.316

SLOVENEC, D. & PALINKAŠ, A.L. (2003): Note in: SLOVENEC, D. & BERMANEC, V. Sistematska mineralogija-mineralogija silikata (Systematic mineralogy- silicate mineralogy), Uni. Zagreb, 359 p.

STEVEN, T. & ZVI, C. (2011): Lithium production from highly saline Dead sea brines.– Rev Chem Engineering, 9/3–4, 293–318.

SZAKALL, S. (2001): Comparison of the Rudabanya (Hungary) and Nižna Slana (Slovakia) metasomatic iron and hydrothermal sulphide ore deposits with special references to the mineral paragenesis of Rudabanja.– Diss, Tech Uni Košice, 154 p.

STRMIĆ PALINKAŠ, S. (2004): Organic and inorganic geochemistry of Ljubija mineral deposits, NW Bosnia.– Master thesis, Uni Zagreb, 101 p.

STRMIĆ PALINKAŠ, S., SPANGENBERG, J.E. & PALINKAŠ A.L. (2009): Organic and Inorganic Geochemistry of Ljubija Siderite Deposits, NW Bosnia and Herzegovina.– Miner Deposita, 44, 893–913.

STIPP, M., STÜNITZ, H., HEILBRONNER, R. & SCHMIDT, S.M. (2002): The eastern Tonale fault zone: a „natural laboratory“ or crystal plastic deformation of quartz over temperature range from 250 to 700ºC.– J Struc Geol, 24, 1861–1884. doi: 10.1016/S0191-8141(02)00035-4

ŠARAC, M. (1981): Metalogenetske karakteristike rudonosne oblasti Ljubije (Metallogenic characteristics of the Ljubija ore-bearing region; in Serbian).– Doc thesis, Uni Belgrade, Belgrade, 135 p.

URBAN, M., THOMAS, R., HURAI, V., KONEČNÝ, K. & CHOVAN, M. (2006): Superdense CO_2 inclusions in Cretaceous quartz-stibnite veins hosted in low-grade Variscan basement of the Western Carpathians, Slovakia.– Miner Deposita, 40, 867–873. Doi: 10.1007/s00126-005-0042-6

VERMA, S.P. & SANTOYOA, E. (1997): New improved equation for Na/K, Na/Li and SiO_2 geothermometers by outlier detection and rejection.– J Volcanol Geoth Res, 79, 9–23.

WARNE, S. ST. J. (1962): A quick field or laboratory staining scheme for the differentiation of the major carbonate minerals.– J Sed Petrol, 32, 29–38.

ZHANG, Y.G. & FRANTZ, J.D. (1987): Determination of the homogenization temperatures and densities of supercritical fluids in the system NaCl−KCl−$CaCl_2$−H_2O using synthetic fluid inclusions.– Chem Geol, 64, 335–350.